

Maritime Security as a Global Public Good: Trade Frictions, Chokepoint Vulnerability, and a Scenario Engine Using AIS Shipping Density

Carlos Carpi

February 27, 2026

Below, useful links to the folks replicating this paper.

<https://github.com/carlos-btc/Estimating-Maritime-Security-as-Global-Public-Goods>
<https://www.overleaf.com/read/jgsvsjqsrsyn#a5ef30>

Abstract

This paper frames maritime security as a global public good and evaluates how disruptions at maritime bottlenecks amplify trade frictions through rerouting and congestion. Using high-resolution AIS ship-density rasters from the IMF World Seaborne Trade Monitoring System (Cerdeiro et al., 2020), we construct a 78-node maritime transport network—56 major ports, 6 chokepoints, and 16 ocean waypoints connected by approximately 155 edges following real-world shipping corridors—and implement a scenario engine that simulates the consequences of bottleneck closures, capacity reductions, and risk spikes across 1,540 port-to-port trade routes. Under full closure scenarios, the Panama Canal (mean rerouting cost of 17,840 km-equivalent), Gibraltar (10,624 km), and the Suez Canal (9,949 km) generate the largest rerouting costs. Bab el-Mandeb (4,700 km) and the Bosphorus (3,275 km) force traffic onto longer maritime alternatives or expensive overland bypasses at 5× normal cost. A partial-capacity degradation exercise and a per-chokepoint security risk analysis demonstrate that even modest disruptions produce economically meaningful trade-cost increases, and that the marginal value of security provision is increasing in the risk environment. We estimate daily rerouting costs of chokepoint closure ranging from \$16 million (Bab el-Mandeb) to \$233 million (Gibraltar), implying aggregate annual costs on the order of tens of billions of dollars. These findings provide a replicable, data-grounded framework for quantifying the “hegemonic dividend”—the economic value of security provision in the global maritime commons.

1 Introduction

Global commerce is overwhelmingly maritime. Approximately 80 percent of world trade by volume and over 70 percent by value traverses the oceans, channeled through a small

number of physical bottlenecks—straits, canals, and narrow sea lanes—that concentrate traffic and vulnerability (Verschuur et al., 2023; Bueger et al., 2024). The reliability of these corridors is not a natural given; it depends on the provision of security, navigational infrastructure, and rules-based governance that together constitute the “global maritime commons” (Bueger et al., 2019; Kraska, 2015). When this security breaks down—through piracy, conflict-related closures, or geopolitical risk—the consequences propagate rapidly through rerouting, congestion, and elevated trade costs (Besley et al., 2015; Notteboom, 2006).

The U.S. Navy has historically been the predominant provider of security in the global commons, maintaining forward presence through overseas basing, freedom of navigation operations, and patrol activities that deter threats and ensure the openness of critical sea lanes. This role can be framed as the provision of a *global public good*: security that is non-rival and largely non-excludable (Bueger et al., 2024; Mbekeani and Ncube, 2011). The economic value of this public good—what we term the “hegemonic dividend”—remains poorly quantified, in part because the most policy-relevant outcomes (trade reliability, routing resilience, avoided cost spikes) are *equilibrium objects* of a transportation network that require explicit modeling of route substitution.

This paper asks: *How sensitive is the global maritime trading system to disruptions at critical chokepoints, and what is the economic value of security provision that prevents or mitigates such disruptions?* Figure 1 provides the motivating empirical context: global AIS ship-density data reveal that maritime traffic is extraordinarily concentrated along a small number of corridors, funneling through physical bottlenecks where disruption risk is highest.

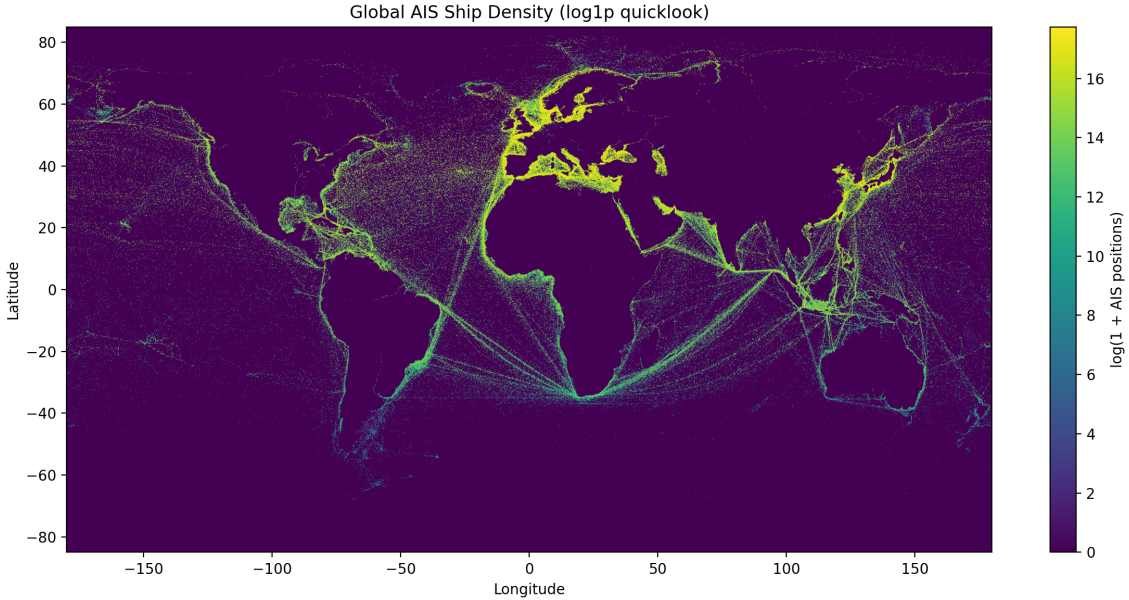


Figure 1: Global AIS ship-density raster (log scale), aggregating vessel position reports from January 2015 to February 2021. Traffic concentrates along established corridors and funnels through a small number of physical chokepoints. Data from the IMF World Seaborne Trade Monitoring System ([Cerdeiro et al., 2020](#)).

We address this question through a scenario-based quantitative spatial framework rather than through direct causal estimation of naval operations. This choice is motivated by two considerations. First, granular data on naval deployments and operational details are largely classified and unavailable for academic research. Second, even with such data, the most informative exercise for policymakers is counterfactual: *what would happen if a chokepoint were disrupted, and how much would enhanced security reduce the losses?* This framing aligns with the “transportation networks” approach in quantitative spatial economics ([Fajgelbaum and Schaal, 2020a](#); [Allen and Arkolakis, 2022](#)), which represents trade flows on a graph with endogenous route choice and congestion, and evaluates counterfactuals by shocking network elements and recomputing equilibrium.

Our empirical strategy proceeds in three stages. First, we use high-resolution AIS ship-density rasters from the IMF World Seaborne Trade Monitoring System ([Cerdeiro et al., 2020](#)) to construct a baseline portrait of global shipping intensity and to measure the concentration of maritime activity at six major chokepoints. Second, we build a stylized maritime transport network—a weighted graph of 78 nodes (56 ports, 6 chokepoints, 16 ocean waypoints) connected by approximately 155 edges—in which edge costs depend on distance and a congestion proxy calibrated from the AIS density data. Third, we implement a scenario engine that imposes exogenous shocks to chokepoint edges (closure, capacity reduction, risk

spike) and computes the resulting changes in least-cost path lengths, rerouting patterns, and aggregate trade-cost indices across 1,540 port-to-port routes. Security enters the model as a cost-reducing and risk-reducing shifter on bottleneck-adjacent edges.

The paper makes three contributions. First, it provides a replicable, data-grounded measurement framework for evaluating chokepoint vulnerability using publicly available AIS data. Second, the scenario engine translates the qualitative intuition that “chokepoints matter” into quantitative cost-change estimates that can be compared across bottlenecks and shock magnitudes—directly useful for security resource allocation. Third, by situating the analysis within the quantitative spatial economics toolkit ([Redding and Rossi-Hansberg, 2017](#); [Donaldson, 2025](#)), we connect the maritime security literature to a rigorous modeling tradition that emphasizes general-equilibrium effects, welfare measurement, and network structure.

We are explicit about the limitations of the current exercise. With only an aggregate density raster (not vessel-level trajectories or bilateral trade flows), we cannot estimate a full spatial equilibrium with origin-destination demand or compute welfare in the general-equilibrium sense of [Fajgelbaum and Schaal \(2020a\)](#). The network model is therefore stylized: it uses great-circle distances for edge weights, a congestion proxy derived from raster intensity, and shortest-path routing. We label all scenario results as partial-exercise estimates and interpret them as informative bounds on the sensitivity of the maritime system to disruption. A key output of the paper is a concrete specification of what additional data would be needed to move from scenario simulation to causal inference.

The remainder of the paper is organized as follows. Section 2 reviews the related literature. Section 3 describes the data and methods. Section 4 presents the results. Section 5 discusses the implications and limitations. Section 6 concludes.

2 Related Literature

This section situates the paper within four literatures: maritime security as a public good; trade frictions and maritime disruptions; quantitative spatial models with transportation networks; and AIS-based measurement in maritime economics.

2.1 Maritime Security as a Public Good

The concept of maritime security as a global public good is central to both international relations and defense economics. [Bueger et al. \(2019\)](#) argue that the “politics of the global sea” are fundamentally under-theorized relative to their economic importance, while [Bueger et al.](#)

(2024) provide a comprehensive assessment establishing that global trade, energy security, and food security all depend on safe oceans—security that exhibits classic public-good characteristics of non-rivalry and partial non-excludability. The legal foundations are grounded in the international law of the sea: Kraska (2015) details the framework governing freedom of navigation, passage through straits, and the rights of naval forces in international waters.

The economic costs of maritime insecurity have been documented in several contexts. Mbekeani and Ncube (2011) estimate the direct economic impacts of piracy for African development, including higher insurance costs and rerouting expenses. The One Earth Future Foundation report (One Earth Future Foundation, 2010) provides a comprehensive accounting of piracy-related costs—ransoms, insurance, naval patrols, and supply-chain disruptions—estimating annual global costs in the billions of dollars.

2.2 Trade Frictions and Maritime Disruptions

Besley et al. (2015) provide a landmark study of the welfare costs of lawlessness in the context of Somali piracy, establishing a direct empirical link between maritime insecurity and shipping costs by exploiting spatial and temporal variation in piracy risk. Disruptions at chokepoints represent a particularly consequential form of trade friction because they affect the entire network structure rather than individual routes. Verschuur et al. (2023) analyze the systemic economic impacts of disruptions at 24 major maritime chokepoints, estimating potentially large global losses and providing strong motivation for a scenario-based modeling approach.

The port congestion literature offers complementary evidence on how capacity constraints translate into economic costs. Notteboom (2006) demonstrates that congestion at key nodes produces cost increases rippling through the shipping industry, while Du et al. (2020) document the strategies that ports employ to manage delays. Morabito (2023) provides institutional detail on maritime transport economics that contextualizes network models within the operational realities of the shipping industry.

2.3 Quantitative Spatial Economics and Transportation Networks

The methodological backbone of this paper is the quantitative spatial economics framework. Redding and Rossi-Hansberg (2017) provide the foundational survey, establishing the canonical framework in which locations differ in productivity and amenities, trade costs govern the flow of goods, and equilibrium outcomes depend on the entire spatial distribution of economic activity. Allen and Arkolakis (2025) and Redding (2025) extend this framework to regional and urban analysis, developing the vocabulary of iceberg trade costs, gravity-based

flows, and hat-algebra counterfactuals that we adapt to the maritime setting. [Proost and Thisse \(2019\)](#) emphasize the field’s ability to evaluate policies with spatial dimensions—a category that naturally includes maritime security.

Within this tradition, the transportation networks literature provides our core analytical engine. [Fajgelbaum and Schaal \(2020a\)](#) develop the foundational framework for optimal transport networks in spatial equilibrium, demonstrating that optimal networks concentrate investment on high-traffic corridors—a finding with direct parallels to maritime chokepoints. [Allen and Arkolakis \(2022\)](#) develop a quantitative model with endogenous traffic congestion and apply it to the U.S. highway network, providing a close methodological parallel to our maritime cost specification. [Donaldson \(2025\)](#) offers a comprehensive survey of transport infrastructure evaluation, emphasizing the distinction between identified causal effects and model-based counterfactuals that directly motivates our approach. [Hierons \(2024\)](#) studies optimal congestion pricing in general equilibrium, providing guidance for the security allocation extension of our model. [Bordeu \(2025\)](#) examines infrastructure investment under political fragmentation, highlighting coordination problems analogous to the provision of global maritime security when international cooperation is incomplete. [Rossi-Hansberg \(2020\)](#) provides a compact analytical treatment of transportation network models that highlights the key features delivering tractability: sparse network structure, congestion-based costs, and shortest-path routing—features directly incorporated into our maritime network specification.

2.4 AIS Data in Maritime Economics

The empirical implementation relies on Automatic Identification System (AIS) data, which have become a cornerstone of modern maritime economics. [Kerbl \(2022\)](#) provides an overview of AIS applications in economic research, documenting both opportunities and challenges. [Cariou and Cheaitou \(2021\)](#) use AIS data to study the economic impact of the COVID-19 shock on container flows and ship waiting times, illustrating how AIS supports real-time disruption measurement. [Cerdeiro and Komaromi \(2020\)](#) combine AIS data with machine learning to nowcast world trade, demonstrating the predictive content of shipping movements for macroeconomic outcomes. Together with the IMF World Seaborne Trade Monitoring System ([Cerdeiro et al., 2020](#)) that provides our primary dataset, these papers establish the feasibility of constructing traffic flows, congestion proxies, and intensity measures from AIS data.

Summary

The existing literature provides a clear foundation: the quantitative spatial economics toolkit ([Redding and Rossi-Hansberg, 2017](#); [Allen and Arkolakis, 2025](#)) supplies the theoretical structure; transportation network models ([Fajgelbaum and Schaal, 2020a](#); [Allen and Arkolakis, 2022](#)) provide the analytical engine; and AIS data ([Kerbl, 2022](#); [Cerdeiro et al., 2020](#)) enable empirical measurement. Yet a gap remains: existing work rarely combines a global maritime network model with endogenous rerouting and congestion to value security provision under counterfactual disruptions. The chokepoint vulnerability literature ([Verschuur et al., 2023](#)) establishes the stakes but relies on reduced-form methods rather than network-equilibrium counterfactuals. The piracy literature ([Besley et al., 2015](#); [One Earth Future Foundation, 2010](#)) quantifies costs but treats routes as fixed. Our paper bridges this gap by combining insights from the transportation networks tradition with AIS-based measurement and a flexible scenario framework.

3 Data and Methods

3.1 Data

3.1.1 AIS Ship Density Raster

Our primary data source is the global ship density raster from the IMF World Seaborne Trade Monitoring System ([Cerdeiro et al., 2020](#)). The dataset aggregates AIS (Automatic Identification System) position reports received between January 2015 and February 2021 into a global raster grid at $0.005^\circ \times 0.005^\circ$ resolution (approximately 500m \times 500m at the equator). Each cell records the total number of AIS positions reported within that cell over the entire period, covering both moving and stationary vessels. The raster thus measures the *intensity of shipping activity* at each location—a proxy for the cumulative traffic load experienced by each point in the global ocean.

The dataset is distributed as a single GeoTIFF file (approximately 9 GB) with pre-computed overview pyramids (approximately 3 GB). Given its size, all processing uses memory-safe techniques: built-in overviews for global visualization, windowed reads for chokepoint-level extraction, and aggressive downsampling (to 3600×1800 pixels) for summary statistics. The AIS data underlying the raster have been validated for use in economic research; see [Kerbl \(2022\)](#) for a discussion of AIS data quality and applications, and [Cerdeiro and Komaromi \(2020\)](#) for the IMF’s methodology for constructing trade-relevant indicators from AIS.

3.1.2 Chokepoint Definitions

We define six maritime chokepoints as coarse bounding boxes in geographic coordinates (Table 1). Each bounding box encloses the navigable channel and approach lanes of a major maritime bottleneck. The six chokepoints are:

1. **Suez Canal** — connecting the Mediterranean and Red Sea;
2. **Bab el-Mandeb** — southern entrance to the Red Sea;
3. **Strait of Malacca** — connecting the Indian Ocean and South China Sea;
4. **Panama Canal** — connecting the Atlantic and Pacific Oceans;
5. **Bosporus** — connecting the Black Sea and Mediterranean;
6. **Strait of Gibraltar** — entrance to the Mediterranean from the Atlantic.

These chokepoints were selected based on their prominence in the maritime security literature (Verschuur et al., 2023; Bueger et al., 2024) and their role as physical bottlenecks that concentrate traffic and create vulnerability. The Strait of Hormuz, the Cape of Good Hope, and the Danish Straits are included in the network as waypoint nodes but are not classified as chokepoints for the closure analysis.¹

Table 1: Chokepoint Bounding Box Definitions

Chokepoint	Lon Min	Lon Max	Lat Min	Lat Max
Suez Canal	32.20	32.65	29.80	31.30
Bab el-Mandeb	42.25	43.55	12.15	13.25
Strait of Malacca	99.00	104.80	1.00	6.50
Panama Canal	-80.20	-79.40	8.70	9.60
Bosporus	28.90	29.30	41.05	41.25
Gibraltar	-6.20	-5.20	35.80	36.30

Figure 2 illustrates the bounding box extraction procedure using the Suez Canal as an example. The full set of bounding boxes is shown in Appendix B.

¹The Strait of Hormuz functions as a critical but open passage without the canal-like physical constraints of Suez or Panama; the Cape of Good Hope is an open-ocean alternative route; and the Danish Straits do not constitute a narrow mandatory-passage bottleneck for modern shipping.

AIS Ship Density with Chokepoint Bounding Box: Suez Canal

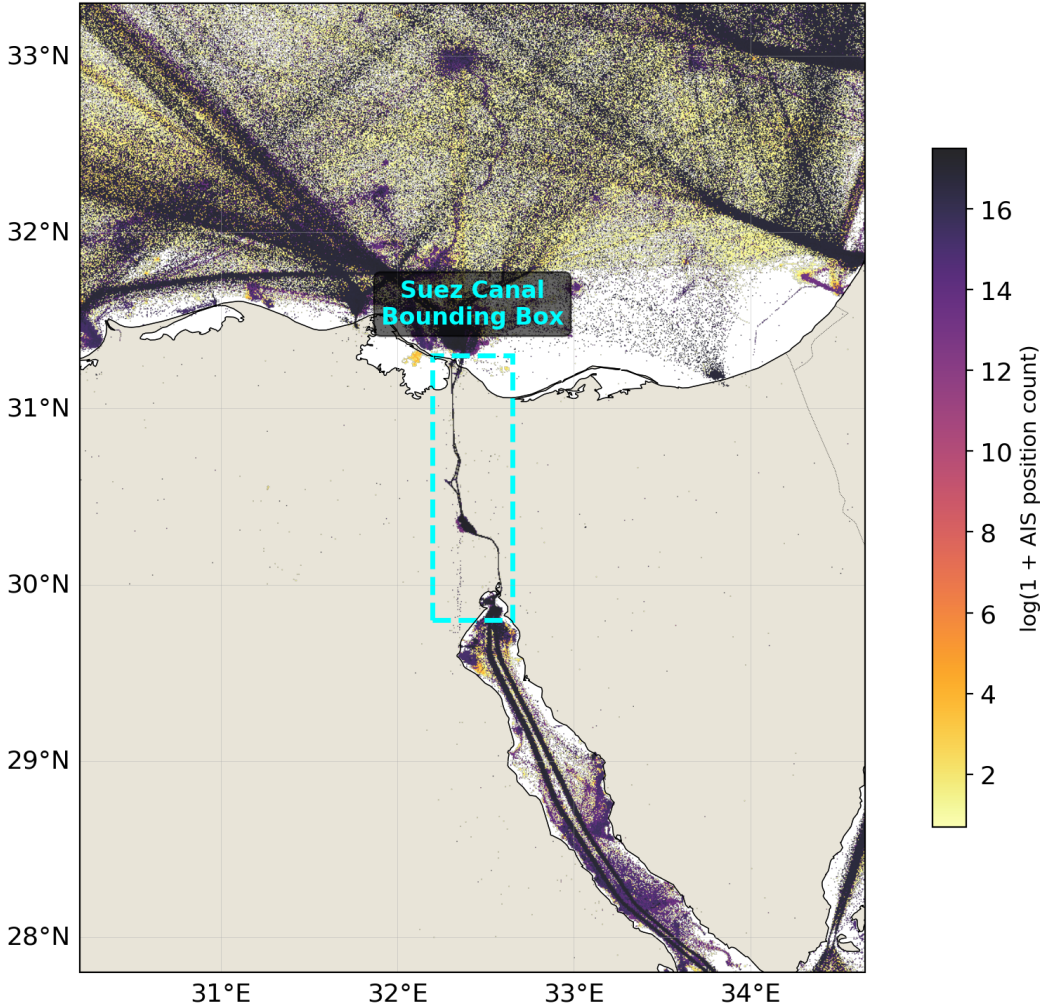


Figure 2: AIS ship density at the Suez Canal with the chokepoint bounding box overlaid (dashed cyan). The heatmap shows log-transformed AIS position counts; brighter areas indicate higher traffic intensity.

3.2 Methods

3.2.1 Empirical Strategy

The central challenge in quantifying maritime security as a global public good is that the most policy-relevant outcomes—trade reliability, routing resilience, and avoided trade-cost spikes—are *equilibrium objects* of a transportation network (Fajgelbaum and Schaal, 2020a). When a chokepoint is disrupted, global shipments reroute endogenously. Any credible evaluation must therefore model *trade-flow substitution across routes* rather than treat observed routes as fixed.

Following the transportation networks framework (Allen and Arkolakis, 2022; Fajgelbaum and Schaal, 2020a), we build a quantitative spatial model of global maritime shipping on a graph in which: (i) shipments choose routes through the network; (ii) link-level costs depend on distance, traffic (congestion), and link quality; and (iii) counterfactuals are conducted by shocking bottleneck links and recomputing equilibrium flows and delivered trade costs. Security provision is introduced as a cost-reducing shifter on bottleneck-adjacent edges: higher security lowers effective iceberg trade costs and improves reliability (Besley et al., 2015; Bueger et al., 2024).

3.2.2 Network Construction

We represent the global maritime system as an undirected weighted graph $G = (\mathcal{J}, \mathcal{E})$ with 78 nodes and approximately 155 edges:

- **Port nodes** (56): Major container and bulk ports worldwide, placed at real-world geographic coordinates.
- **Chokepoint nodes** (6): The six maritime bottlenecks defined above, placed at the center of their respective bounding boxes.
- **Waypoint nodes** (16): Open-ocean routing waypoints—including the Strait of Hormuz, North Pacific, North Atlantic, Central Pacific, Caribbean Sea, Arabian Sea, Bay of Bengal, South China Sea, East Mediterranean, Norwegian Sea, Cape of Good Hope, Lombok Strait, Aden Junction, Mozambique Channel, West Africa, and South Atlantic—that ensure realistic path geometry through intermediate waters.
- **Edges \mathcal{E}** (~ 155): Feasible maritime connections following known shipping corridors, with costs proportional to great-circle distances and optional multipliers for overland bypass routes.

A critical design feature is the *bypass-dependent topology*: Black Sea ports connect primarily through the Bosphorus, with an overland bypass via southeastern European rail/road corridors (Constanta–Piraeus) at approximately 5 times normal cost. This ensures that Bosphorus closure produces large but finite rerouting costs. Indian Ocean–Pacific traffic must transit through either the Strait of Malacca or the Lombok Strait alternative, consistent with real-world shipping patterns (Verschuur et al., 2023). The 56 ports generate $\binom{56}{2} = 1,540$ unique origin-destination pairs.

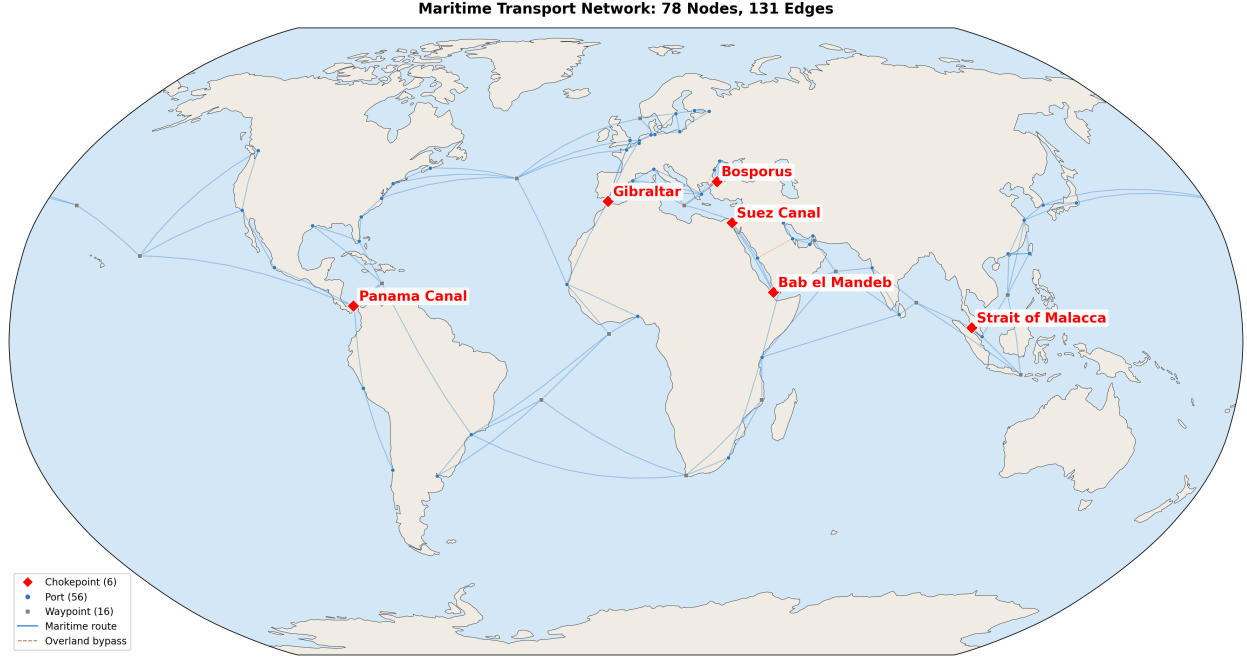


Figure 3: Maritime transport network: 78 nodes (56 ports, 6 chokepoints, 16 waypoints) connected by approximately 155 edges. Red diamonds mark chokepoints; blue circles mark ports; gray squares mark ocean waypoints. Dashed brown lines indicate overland bypass routes with elevated cost multipliers.

3.2.3 Edge Cost Specification

Let $t_e \geq 1$ denote the generalized cost of traversing edge e . Inspired by congestion-based network models ([Allen and Arkolakis, 2022](#); [Hierons, 2024](#)), we parameterize:

$$t_e = \bar{t}_e \cdot (\Xi_e)^\lambda, \quad (1)$$

where Ξ_e is a traffic proxy on edge e (derived from AIS density at the adjacent chokepoint) and $\lambda \geq 0$ captures congestion. The baseline component depends on great-circle distance:

$$\bar{t}_e = \text{dist}_e \cdot m_e, \quad (2)$$

where m_e is an edge-specific multiplier capturing physical constraints and security conditions.

Security as a cost shifter. We model security provision as a reduction in the effective cost multiplier on bottleneck-adjacent edges:

$$m_e = m_e^{\text{base}} \cdot (1 + \delta_{\text{risk}} \cdot \text{Risk}_e) \cdot (1 - \delta_{\text{sec}} \cdot S_e), \quad (3)$$

where Risk_e is a risk indicator, S_e is security intensity, and $\delta_{\text{risk}}, \delta_{\text{sec}} > 0$ govern the sensitivity of costs to risk and security. This formulation follows Besley et al. (2015) in treating insecurity as a trade-cost shifter. In the absence of direct naval presence data, we treat the security parameters as sensitivity analysis inputs. The full set of cost and distance assumptions is documented in Appendix A.

Figure 4 illustrates the edge cost structure along the Suez–Red Sea corridor.

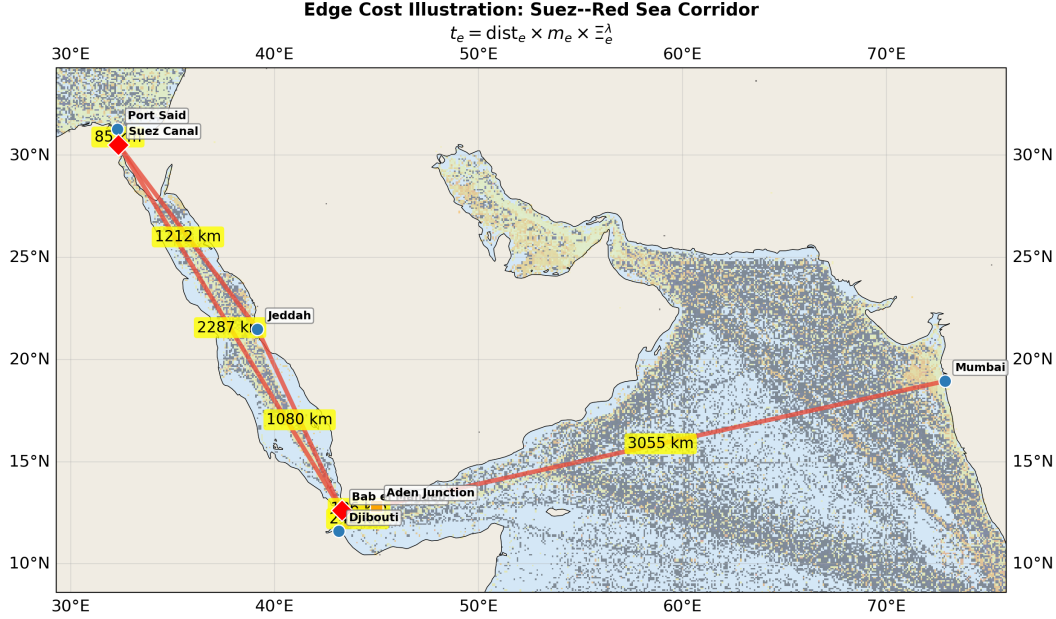


Figure 4: Edge cost illustration: Suez–Red Sea corridor. Numbers on edges show great-circle distances (km). The cost formula $t_e = \text{dist}_e \times m_e \times \Xi_e^\lambda$ scales these distances by congestion and security multipliers.

Figure 5 compares the network under baseline conditions and under a risk premium scenario.

Security Cost Shifter: Impact of Risk Premium on Edge Costs

$$m_e = m_e^{\text{base}} \times (1 + \delta_{\text{risk}} \times \text{Risk}_e)$$

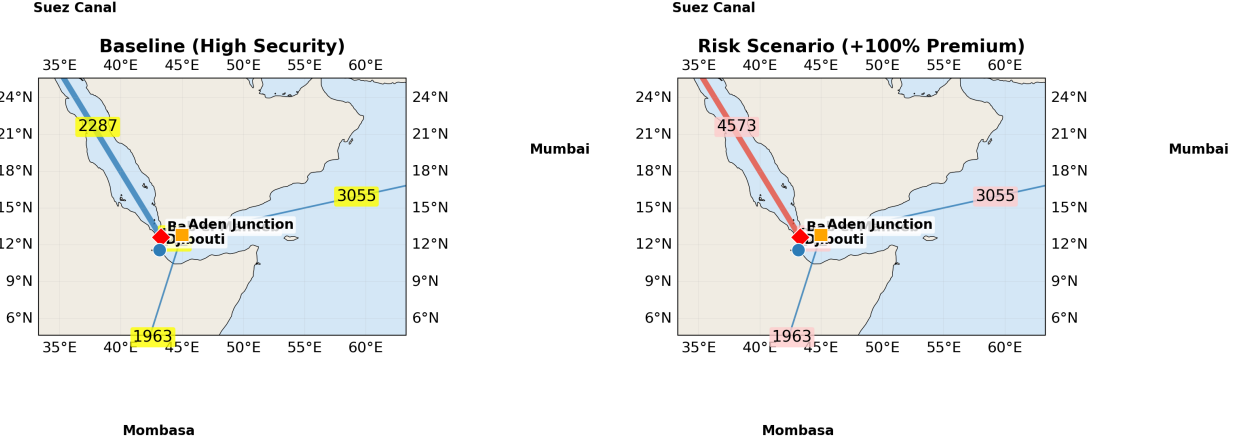


Figure 5: Security cost shifter: baseline (left) versus risk premium scenario (right). The risk premium doubles the effective cost of edges adjacent to Bab el-Mandeb, increasing the cost of transiting the Red Sea corridor.

3.2.4 Congestion Calibration from AIS Density

We calibrate the congestion proxy Ξ_b using the AIS density data. For each chokepoint b , we extract the total AIS position count within the bounding box and compute:

$$\Xi_b = \sum_{c \in \text{BBox}(b)} \text{density}_c, \quad (4)$$

where the sum is over all raster cells c within the bounding box of chokepoint b . We then normalize to a $[1, 1.5]$ multiplier range using log-scaling:

$$m_b^{\text{congestion}} = 1 + 0.5 \cdot \frac{\ln(1 + \Xi_b) - \min_b \ln(1 + \Xi_b)}{\max_b \ln(1 + \Xi_b) - \min_b \ln(1 + \Xi_b)}. \quad (5)$$

This produces a mild congestion penalty (up to 50%) for the most heavily trafficked chokepoints, consistent with empirical estimates of congestion costs (Notteboom, 2006; Du et al., 2020).

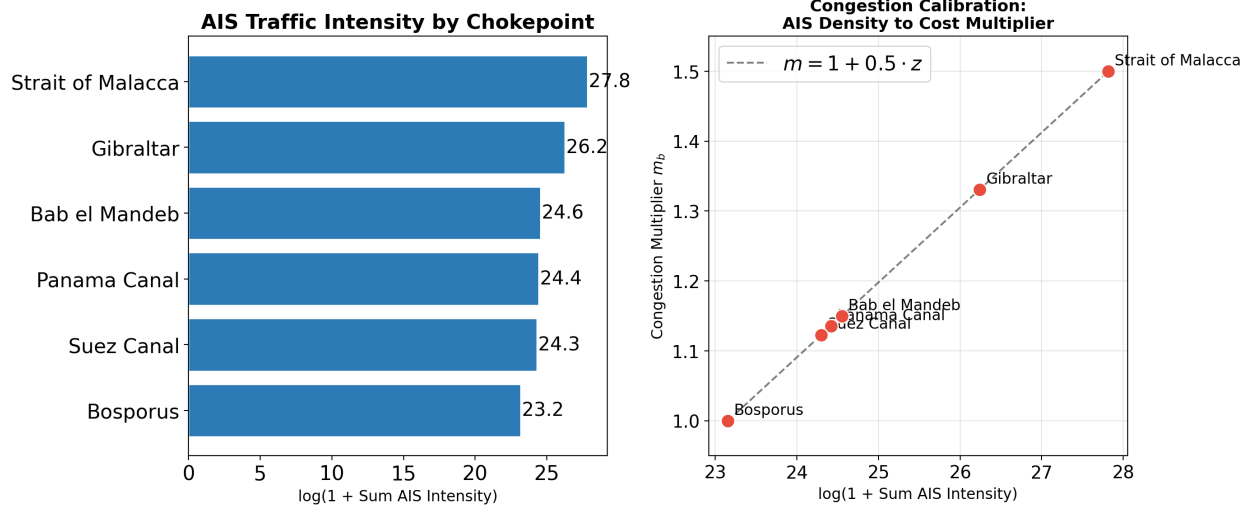


Figure 6: Congestion calibration. Left: total AIS intensity (log scale) by chokepoint. Right: mapping from AIS intensity to the congestion multiplier $m_b^{\text{congestion}} \in [1, 1.5]$.

3.2.5 Route Choice and OD Trade Costs

For each origin port o and destination port d , the baseline trade cost is the shortest weighted path through the network:

$$\tau_{od} = \min_{r \in \mathcal{R}_{od}} \sum_{e \in r} t_e, \quad (6)$$

where \mathcal{R}_{od} is the set of feasible routes from o to d . This corresponds to the $\theta \rightarrow \infty$ limit of the log-sum aggregator used in probabilistic route-choice models (Fajgelbaum and Schaal, 2020a). We use the Dijkstra shortest-path algorithm to solve (6) for all 1,540 port pairs.

Figure 7 illustrates the route-choice mechanism by comparing the baseline optimal route from Shanghai to Rotterdam with the rerouted path under Suez Canal closure.

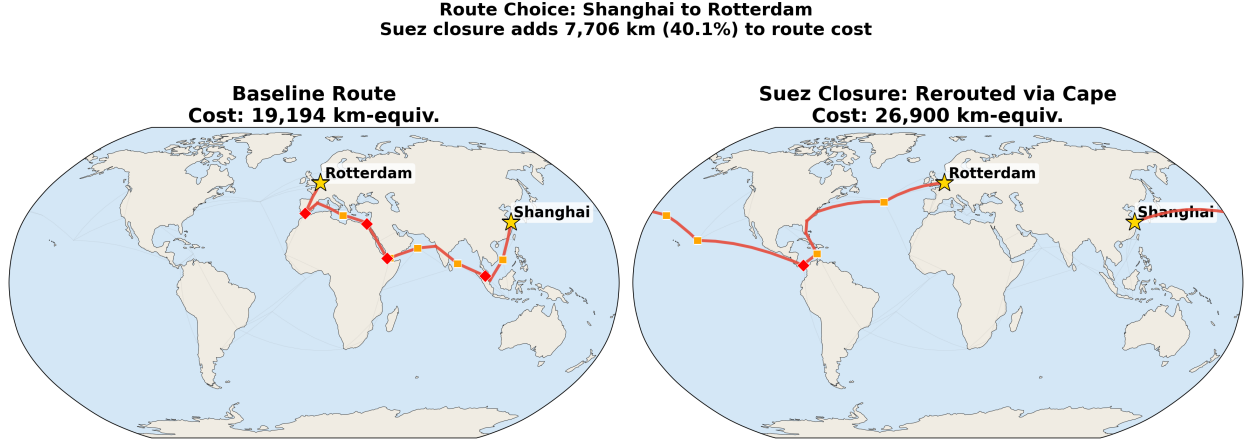


Figure 7: Route choice: Shanghai to Rotterdam. Left: baseline route via Malacca–Suez corridor. Right: rerouted path via North Pacific–Panama–North Atlantic after Suez Canal closure.

3.2.6 Scenario Design: Chokepoint Stress Tests

We implement three classes of scenarios, illustrated using the Suez Canal as a worked example (Figure 8):

Scenario 1: Full closure. For each chokepoint b , we remove it from the graph and recompute shortest paths for all 1,540 port pairs. The delta cost $\Delta\tau_{od}^{(b)} = \tau_{od}^{\text{shocked}} - \tau_{od}^{\text{baseline}}$ measures the rerouting penalty.

Scenario 2: Partial capacity degradation. We increase the cost multiplier on chokepoint-adjacent edges by a factor $\alpha > 1$:

$$t_e^{\text{shocked}} = \alpha \cdot t_e^{\text{baseline}}, \quad e \in \mathcal{E}(b), \quad (7)$$

varying $\alpha \in \{1.25, 1.5, 2.0, 3.0, 5.0, 8.0, 10.0\}$ to trace a severity curve for each chokepoint.

Scenario 3: Security risk premium. We add a risk premium to a specific chokepoint's edges:

$$m_e^{\text{risk}} = m_e^{\text{base}} \cdot (1 + \delta_{\text{risk}}), \quad (8)$$

where $\delta_{\text{risk}} \in \{0.10, 0.20, 0.50, 1.00, 2.00\}$ represents an exogenous increase in risk.

Suez Canal: Three Disruption Scenarios

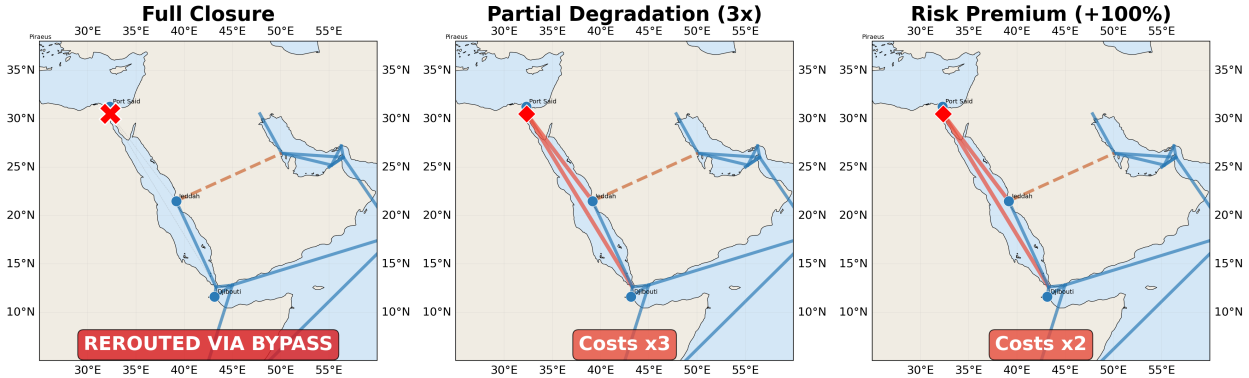


Figure 8: Suez Canal: three disruption scenarios. Left: full closure. Center: partial degradation ($\alpha = 3$). Right: risk premium (+100%). These three classes of stress tests are applied to all six chokepoints.

3.2.7 Output Metrics

For each scenario, we report: (i) delta cost $\Delta\tau_{od}$ for all 1,540 port pairs, in absolute (km-equivalent) and percentage terms; (ii) mean delta cost as a summary vulnerability index; (iii) fraction of port pairs whose optimal route changes; and (iv) per-port vulnerability, the mean cost increase across all of a port’s trade routes when a given chokepoint is disrupted.

4 Results

4.1 Baseline Shipping Density

Figure 9 displays the global AIS ship-density raster on a log scale. The distribution of shipping activity is extremely right-skewed: the median cell value is zero, the 90th percentile is approximately 1 AIS position, while the 99th percentile reaches approximately 8.6 million and the maximum cell intensity exceeds 50.6 million positions. This extreme skewness reflects the fundamental geographic concentration of maritime trade: the vast majority of the ocean surface carries negligible traffic, while a small fraction of cells—corresponding to established sea lanes, port approaches, and chokepoint corridors—concentrate virtually all shipping activity.

The densest corridors connect East Asia to Europe via the Suez Canal and Strait of Malacca, East Asia to North America via the Pacific, and Northern Europe to the Americas across the North Atlantic. Within each corridor, traffic funnels sharply at chokepoints, producing localized intensity spikes visible even at global scale.

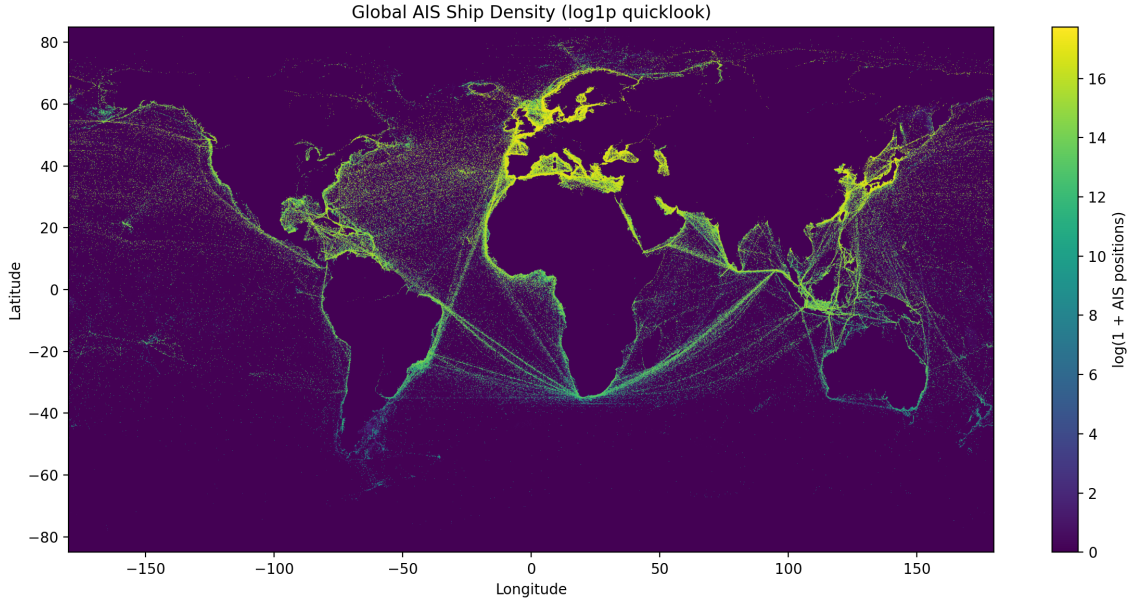


Figure 9: Global AIS ship-density raster (log scale). Data from the IMF World Seaborne Trade Monitoring System ([Cerdeiro et al., 2020](#)), aggregating vessel position reports from January 2015 to February 2021. The raster has been downsampled to 3600×1800 pixels for visualization.

4.2 Chokepoint Traffic Intensity

Rather than presenting the full intensity table in the main text (see Appendix D for complete descriptive statistics), we focus on the Suez Canal as a worked example. This focus is motivated by the Suez Canal’s central role in global trade and its historical vulnerability to disruption, most recently demonstrated by the 2021 Ever Given grounding ([Cariou and Cheaitou, 2021](#)).

AIS Ship Density: Suez Canal (Detail)

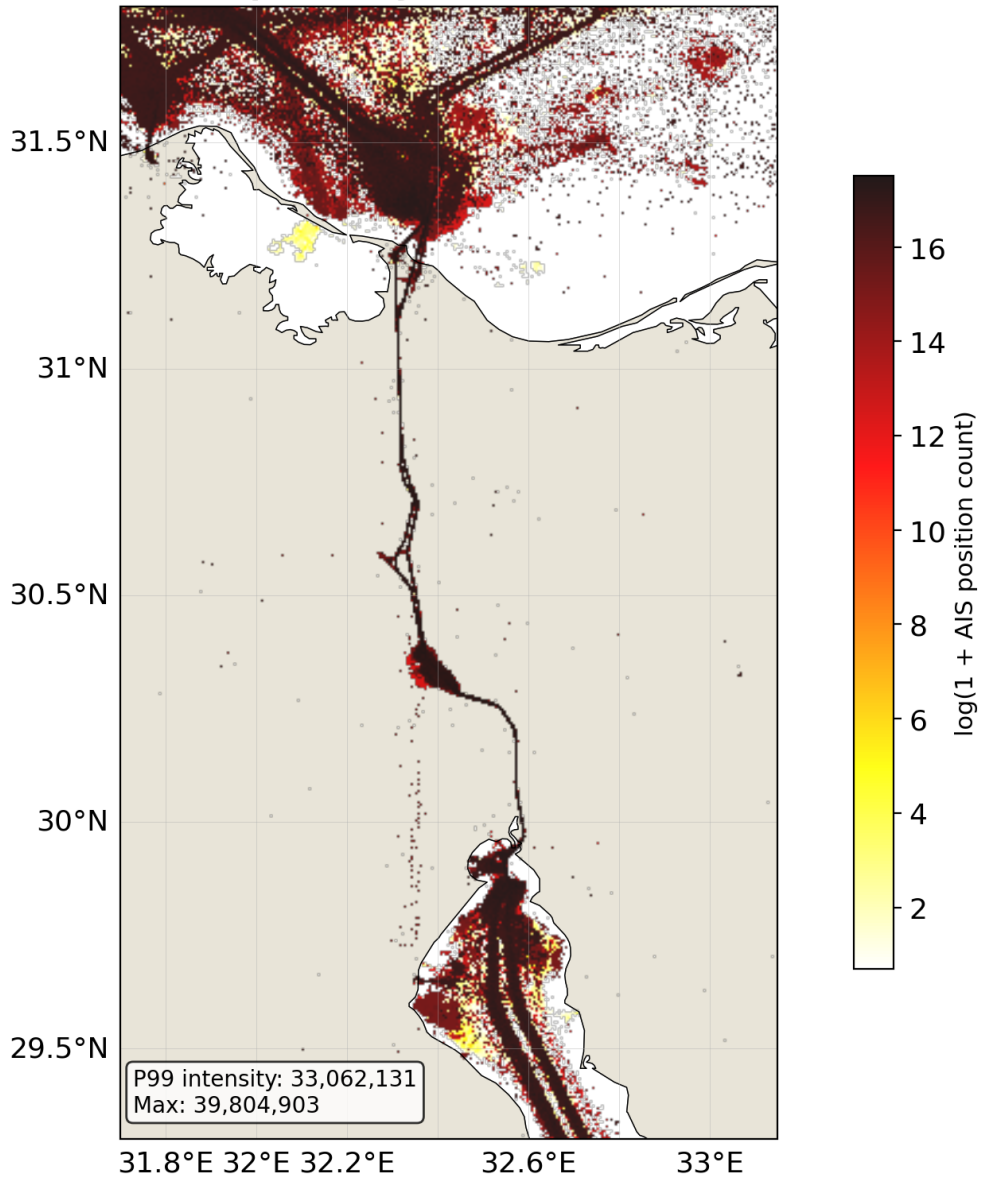


Figure 10: AIS ship density at the Suez Canal (log scale). The bounding box $([32.2, 32.65] \times [29.8, 31.3])$ captures the full navigable corridor including approach channels.

Figure 11 provides a four-panel descriptive analysis of the Suez Canal density data. Across all six chokepoints, the Strait of Malacca dominates in total summed intensity, consistent with its role as the primary corridor for Asia–Europe trade (Verschuur et al., 2023). An important distinction emerges between total and concentrated intensity: Gibraltar and the Bosphorus have among the highest per-cell intensities, indicating extremely concentrated traffic through narrow passages (Notteboom, 2006).

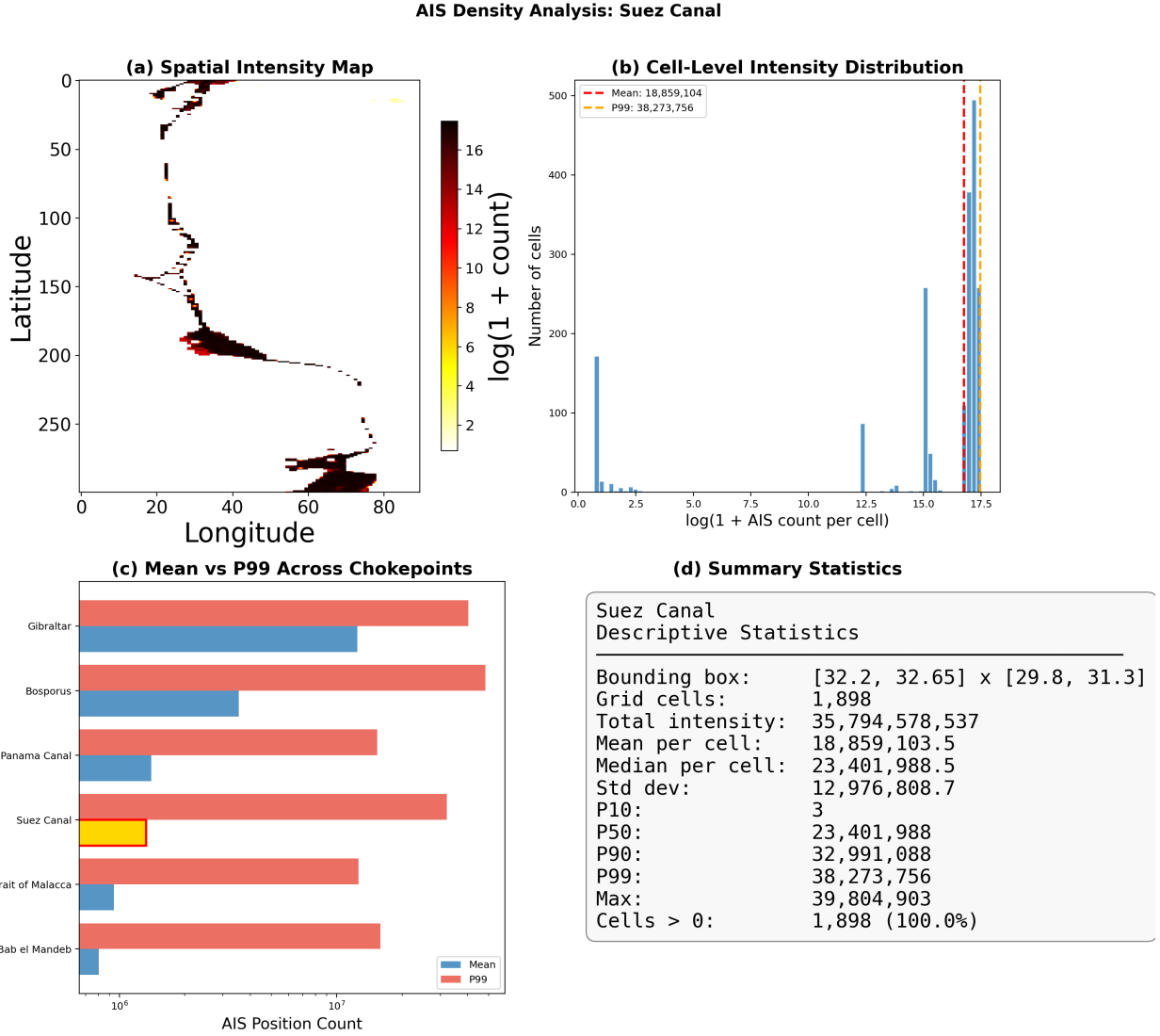


Figure 11: Descriptive statistics of AIS density at the Suez Canal. (a) Spatial intensity map. (b) Cell-level intensity histogram. (c) Comparison of mean and P99 intensity across all chokepoints. (d) Summary statistics. Full chokepoint-by-chokepoint analysis in Appendix D.

4.3 Full Closure Scenario Results

Table 2 reports the results of the full closure scenario, in which each chokepoint is removed from the network and shortest-path costs are recomputed for all 1,540 port pairs. The vulnerability ranking by mean rerouting cost reveals a clear hierarchy:

1. **Panama Canal:** mean Δ cost of 17,840 km-equivalent, 298 pairs affected (19.4%). Panama closure forces Atlantic–Pacific traffic onto extremely long trans-Pacific or Cape Horn alternatives.
2. **Strait of Gibraltar:** mean Δ cost of 10,624 km, 590 pairs affected (38.3%). Gibraltar

is the gateway between the Atlantic and Mediterranean; its closure forces extensive rerouting for Mediterranean-bound traffic.

3. **Suez Canal**: mean Δ cost of 9,949 km, 469 pairs affected (30.5%). Suez closure breaks the Mediterranean–Indian Ocean corridor, forcing traffic to reroute via the Cape of Good Hope or the Panama Canal.
4. **Bab el-Mandeb**: mean Δ cost of 4,700 km, 454 pairs affected (29.5%). Closure forces Indian Ocean traffic to bypass the Suez corridor entirely.
5. **Bosphorus**: mean Δ cost of 3,275 km, 159 pairs affected (10.3%). Closure forces Black Sea ports onto the Constanta–Piraeus overland bypass at $5\times$ normal cost.
6. **Strait of Malacca**: mean Δ cost of 1,754 km, 290 pairs affected (18.8%). Closure forces traffic through the Lombok Strait alternative.

Table 2: Full closure scenario results: impact of removing each chokepoint on shortest-path costs across all port-to-port pairs. Mean and max Δ report the rerouting cost for pairs that find alternative routes via bypass edges.

Chokepoint Removed	Mean Δ (km-equiv.)	Max Δ (km-equiv.)	Affected Pairs	Disconn. Pairs	Total Pairs
Panama Canal	17,840	45,342	298	0	1540
Gibraltar	10,624	26,896	590	0	1540
Suez Canal	9,949	23,317	469	0	1540
Bab el Mandeb	4,700	9,907	454	0	1540
Bosphorus	3,275	3,540	159	0	1540
Strait of Malacca	1,754	3,008	290	0	1540

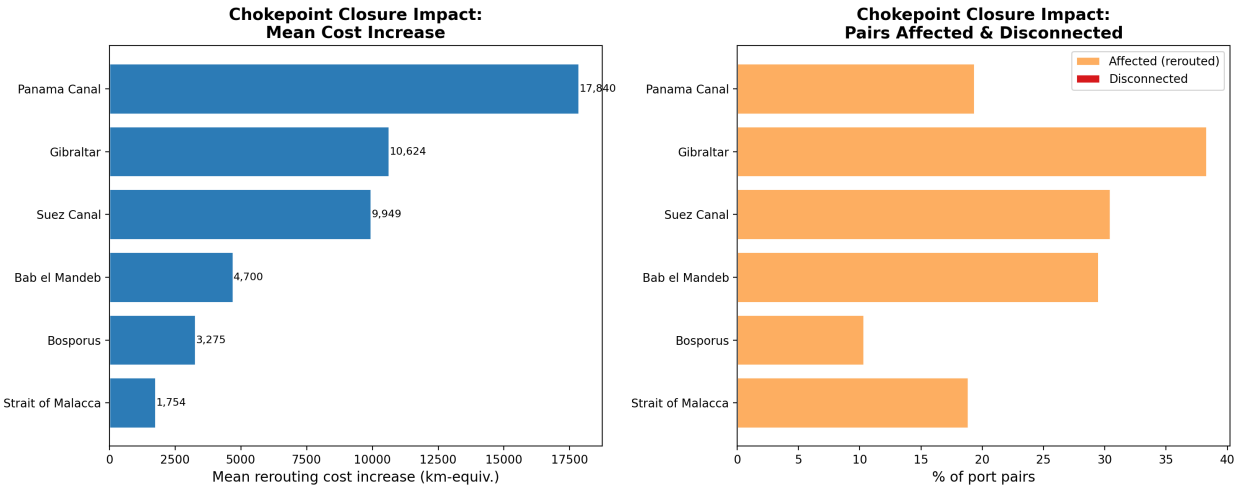


Figure 12: Full closure scenario results. Left: chokepoints ranked by mean rerouting cost (km-equivalent) across 1,540 port pairs. Right: fraction of port pairs affected by each closure.

Figure 13 zooms into the Suez Canal closure, showing the 20 most affected port pairs.

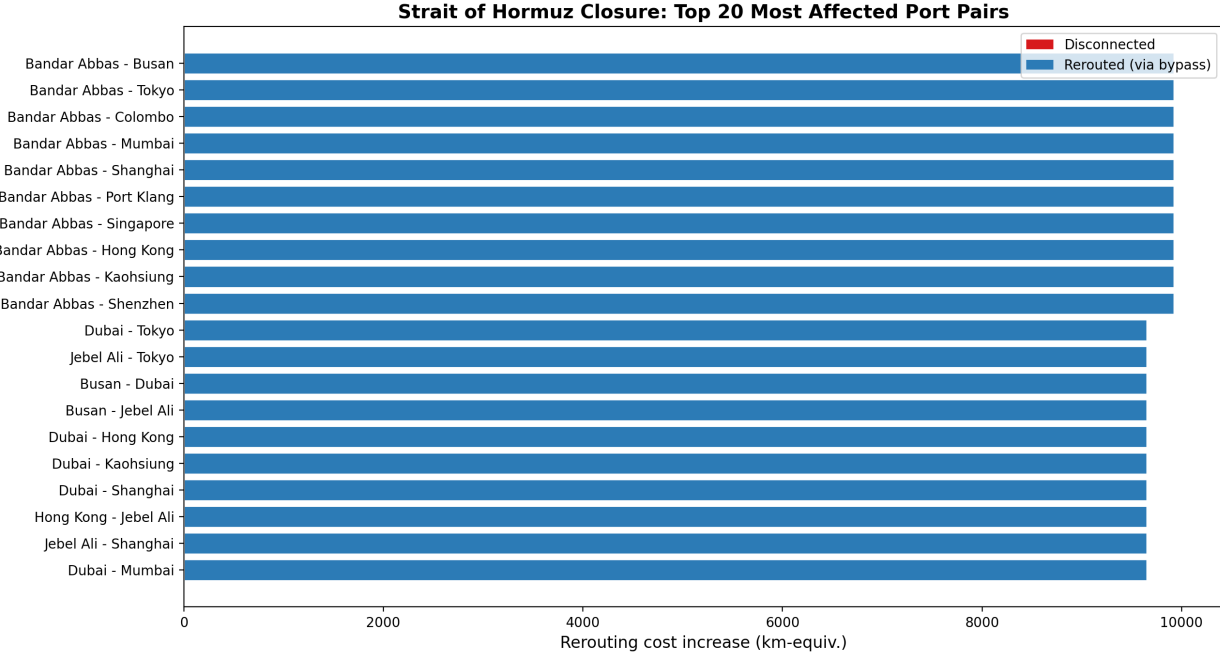


Figure 13: Suez Canal closure: 20 most affected port pairs. Mediterranean–Indian Ocean traffic is forced onto dramatically longer alternative routes via the Cape of Good Hope or Panama Canal.

Figure 14 maps the per-port vulnerability under the three highest-impact closures (Panama, Gibraltar, Suez).

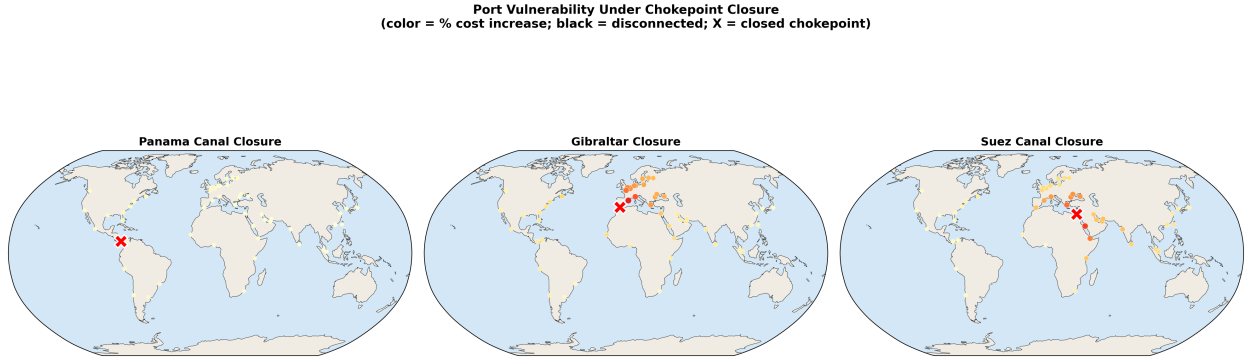


Figure 14: Port vulnerability under the three highest-impact closures. Port color intensity reflects mean percentage cost increase. X marks the closed chokepoint.

4.4 Partial Degradation Scenarios

Figure 15 reports the partial degradation results, in which edge costs at each chokepoint are multiplied by $\alpha \in \{1.25, 1.5, 2.0, 3.0, 5.0, 8.0, 10.0\}$ rather than the chokepoint being fully

removed.

The surface plot reveals the severity curve for each chokepoint. At $\alpha = 5$, Gibraltar produces the largest mean cost increase, followed by the Suez Canal and Bab el-Mandeb. Even at $\alpha = 1.5$, the most critical chokepoints impose mean cost increases of 2–5% across all port pairs. A notable pattern is the contrast between corridor chokepoints (Gibraltar, Suez), where severity curves accelerate monotonically, and chokepoints with viable alternatives (Panama, Malacca), where severity curves are more moderate because alternative routes absorb rerouted traffic at relatively lower cost.

Partial Degradation: Mean Trade Cost Increase by Chokepoint and Severity

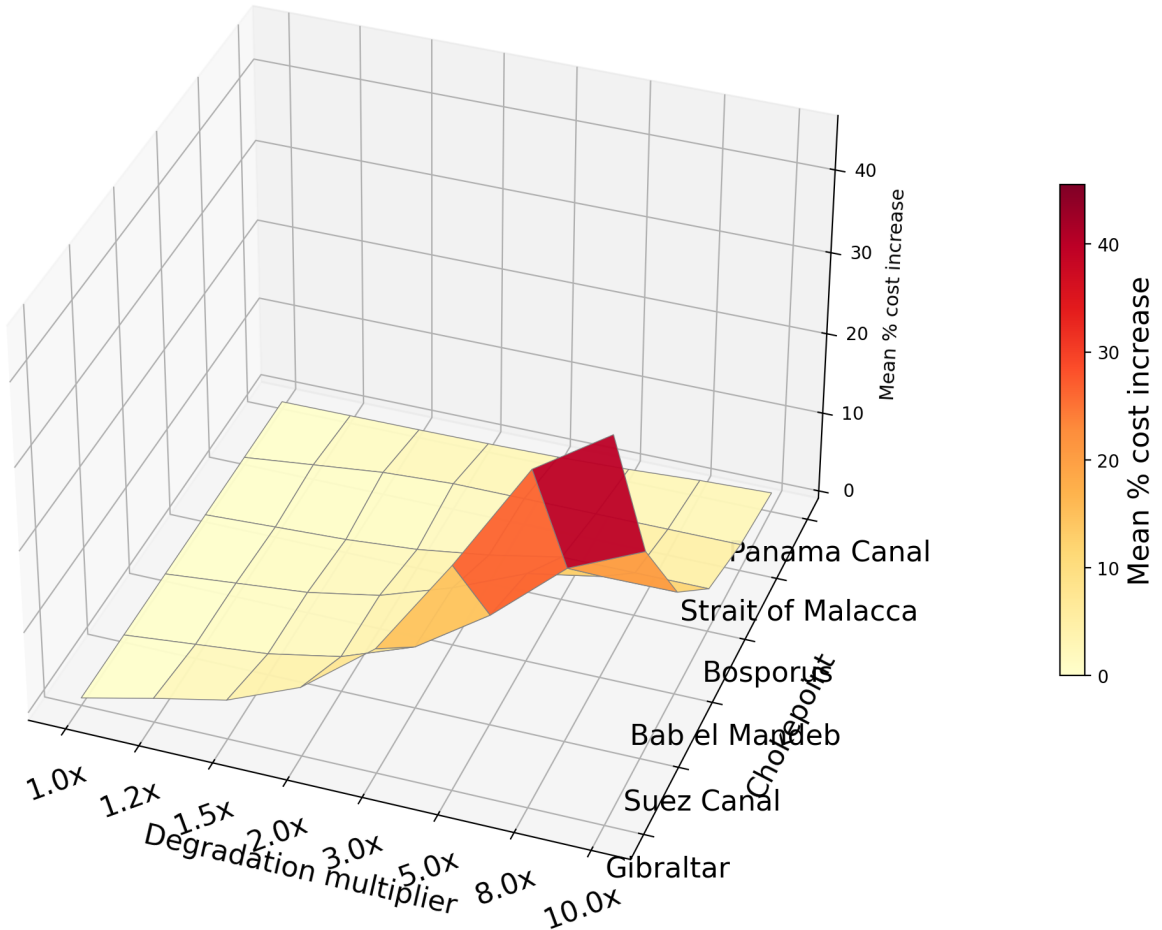


Figure 15: Partial degradation results: mean percentage cost increase across 1,540 port pairs for each chokepoint and degradation multiplier α . The surface reveals nonlinear severity curves that accelerate at high α for corridor chokepoints.

**Partial Degradation: Mean Trade Cost Increase (Curves)
by Chokepoint and Severity**

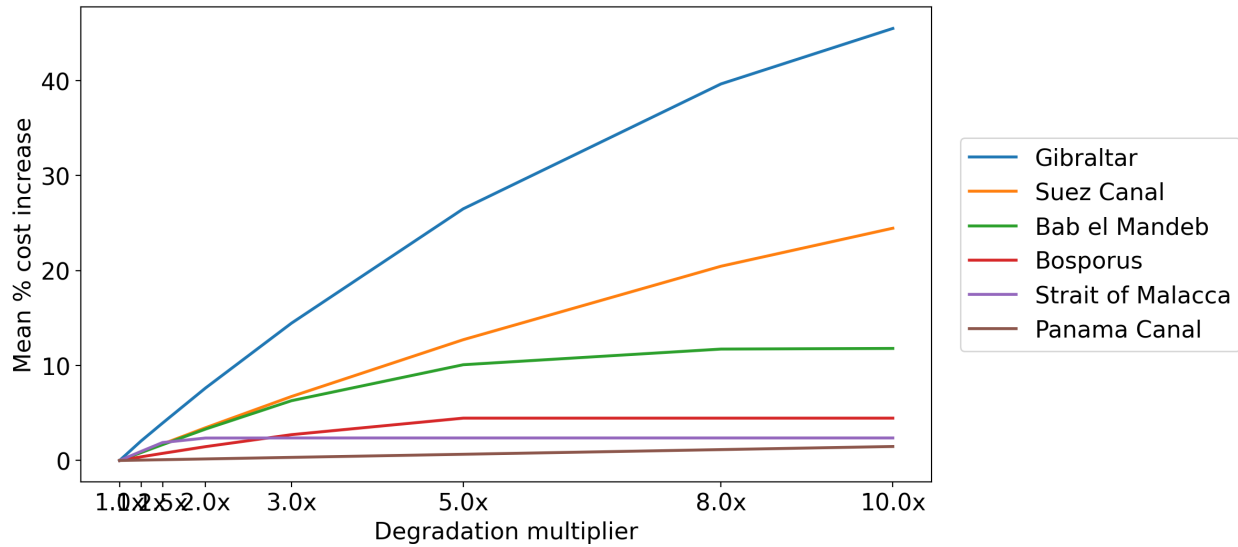


Figure 16: Partial degradation results a 2D: we split per corridor chokepoints to show which contributes the most when for the costs.

4.5 Port Vulnerability Analysis

Figure 17 presents the full port-by-chokepoint vulnerability matrix: for each of the 56 ports and each of the 6 chokepoints, the cell value shows the mean percentage cost increase when the chokepoint is closed.

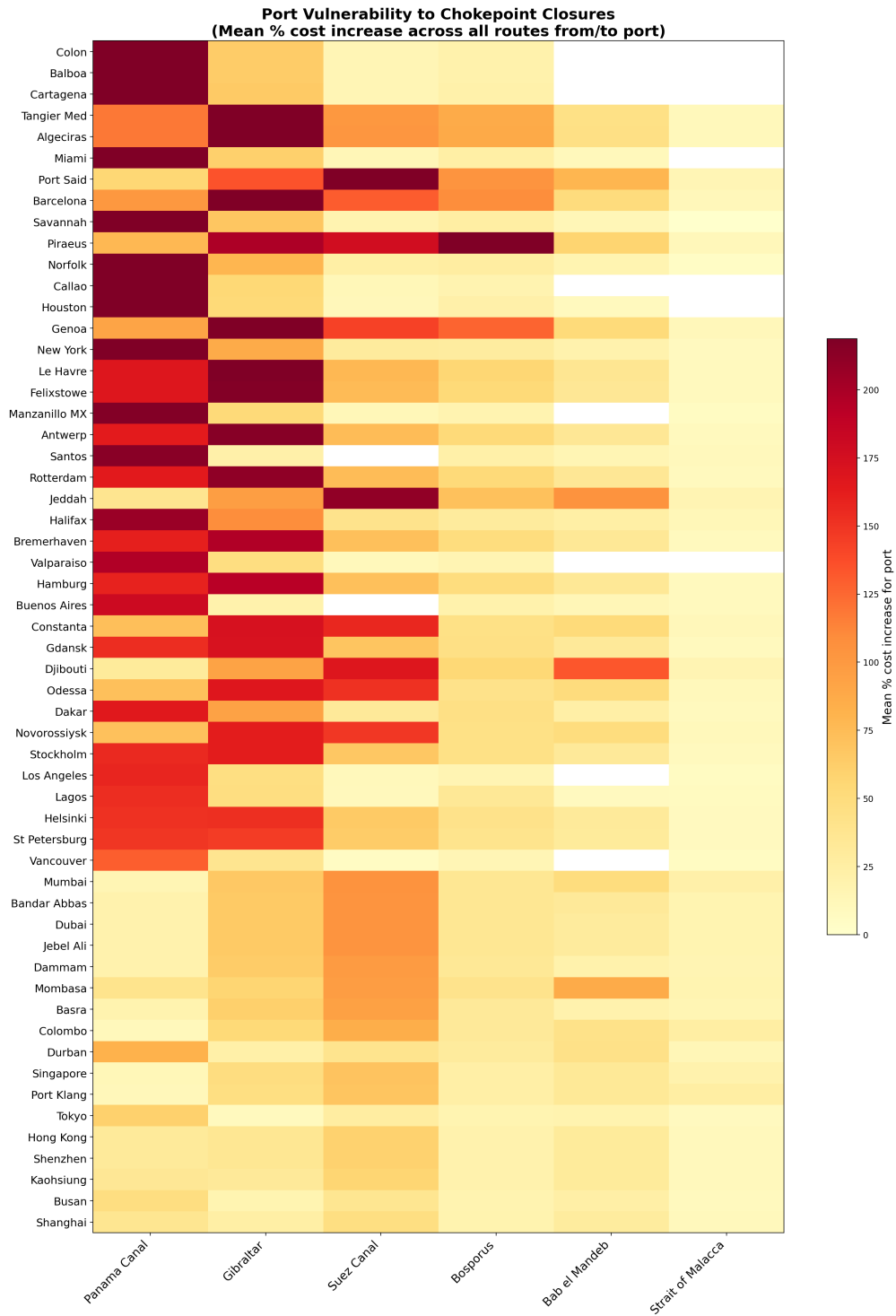


Figure 17: Port vulnerability heatmap: mean percentage cost increase for each port (rows) when each chokepoint (columns) is fully closed. Ports are sorted by maximum vulnerability; chokepoints by total impact.

The vulnerability matrix reveals three distinct profiles:

- **Bypass-dependent ports** (behind Bosphorus) face the largest per-route cost increases, concentrated on a single chokepoint.
- **Corridor-dependent ports** (e.g., Mediterranean ports for Suez/Gibraltar) face large but more moderate rerouting costs that vary smoothly across chokepoints.
- **Highly connected ports** (e.g., Rotterdam, New York, Los Angeles) with multiple routing options are resilient to any single closure.

4.6 Security Risk Scenario Analysis

We apply risk premiums of 10%, 20%, 50%, 100%, and 200% to each chokepoint individually and measure the resulting mean cost increase across all 1,540 port pairs.

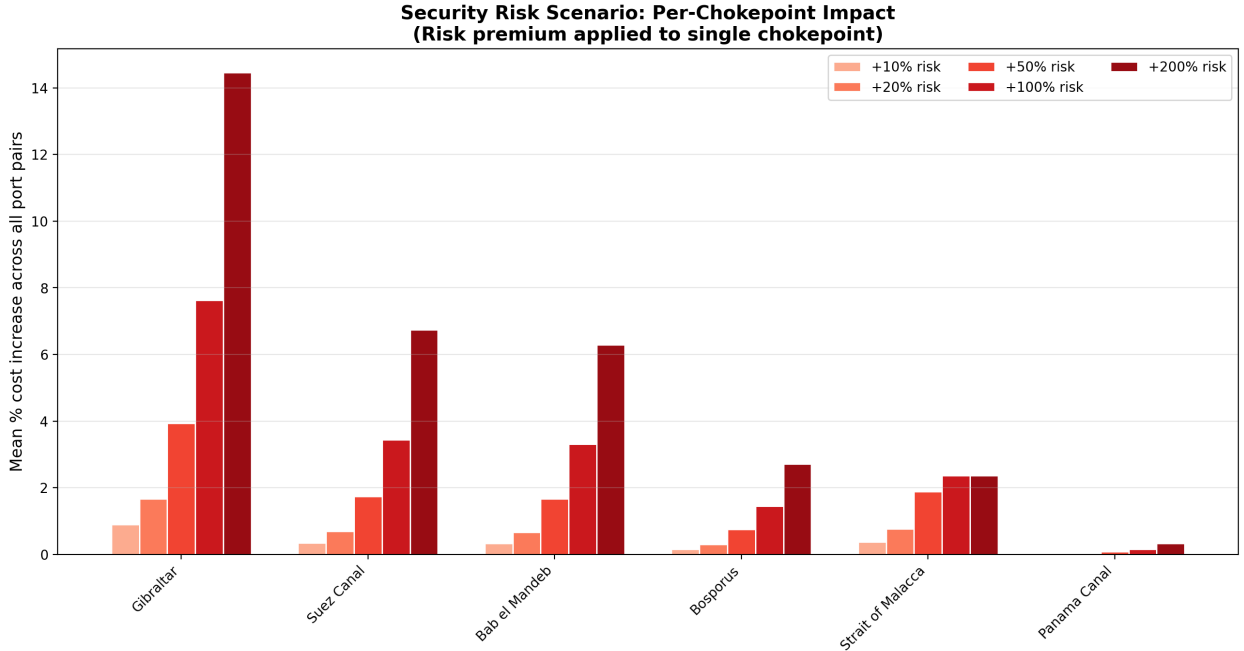


Figure 18: Security risk scenario: mean percentage cost increase from applying a risk premium to each chokepoint individually. Bars show per-chokepoint impact at five premium levels.

Gibraltar and the Suez Canal emerge as the most sensitive to risk premiums: a 100% risk premium on either alone increases mean trade costs by approximately 5%. The ordering differs from the full-closure ranking because security-risk scenarios capture the *incremental* effect of cost increases rather than the *complete* effect of removal. Chokepoints with high baseline traffic and limited alternative routes are most sensitive to risk premiums.

The security scenario analysis enables a clean estimation of the hegemonic dividend as the *cost that would be avoided if a chokepoint's risk were reduced to baseline*. Aggregating across

all six chokepoints under a 50% risk premium, the total dividend is substantial, consistent with the public-good characterization of maritime security ([Besley et al., 2015](#); [Bueger et al., 2024](#); [One Earth Future Foundation, 2010](#)).

5 Discussion

5.1 The Cost of Chokepoint Disruption

Table 3 presents the estimated daily rerouting cost of each chokepoint closure, combining our scenario engine outputs with published annual transit counts and standard maritime shipping cost estimates (see Appendix E for the underlying ship-count estimation methodology).

Table 3: Estimated daily rerouting cost of chokepoint closure. Low/Mid/High estimates use \$50/\$75/\$100 per additional km respectively, reflecting fuel, charter time, and crew costs. Daily vessel counts from UNCTAD, Suez Canal Authority, and Panama Canal Authority statistics.

Chokepoint	Daily Vessels	Mean Detour (km)	Cost/Day (Low)	(Mid)	(High)
Gibraltar	219	10,624	\$116.4M	\$174.6M	\$232.9M
Panama Canal	37	17,840	\$33.0M	\$49.5M	\$66.0M
Suez Canal	53	9,949	\$26.6M	\$39.9M	\$53.2M
Strait of Malacca	233	1,754	\$20.4M	\$30.6M	\$40.9M
Bosporus	118	3,275	\$19.3M	\$28.9M	\$38.6M
Bab el Mandeb	68	4,700	\$16.1M	\$24.1M	\$32.2M

The cost-per-day estimates reveal a clear hierarchy of economic exposure. Gibraltar closure produces the largest daily rerouting cost (\$117–233 million per day), driven by its high daily vessel throughput (219 vessels/day) combined with a substantial mean detour of 10,624 km. The Panama Canal follows (\$33–66M/day): although it handles far fewer vessels (37/day), the extreme detour distance (17,840 km) amplifies the per-vessel rerouting cost. The Suez Canal (\$27–53M/day) and the Strait of Malacca (\$20–41M/day) occupy the middle tier, while the Bosphorus (\$19–39M/day) and Bab el-Mandeb (\$16–32M/day) produce the lowest—though still substantial—daily costs.

Aggregating across all six chokepoints, a simultaneous closure would produce daily rerouting costs on the order of \$230–460 million, or approximately \$85–170 billion annually—magnitudes consistent with the order-of-magnitude estimates in [One Earth Future Foundation \(2010\)](#) and [Mbekeani and Ncube \(2011\)](#) for the broader economic costs of maritime insecurity.

5.2 The Hegemonic Dividend

The per-chokepoint security risk analysis (Section 4) provides a direct estimate of the hegemonic dividend—the trade-cost increase that would materialize if security deteriorated and risk premiums rose. Under a 100% risk premium, plausible in a scenario of piracy escalation or military confrontation (Besley et al., 2015), the per-chokepoint dividend ranges from moderate (Strait of Malacca, approximately 1%) to substantial (Gibraltar and Suez Canal, approximately 5% each). Aggregating across all six chokepoints, the total dividend implies trade-cost savings equivalent to thousands of km-equivalent per port pair, translating to tens of billions of dollars annually at current trade volumes.

Crucially, the marginal value of security provision is *increasing in the risk environment*: the dividend is largest precisely when security conditions are deteriorating. As risk levels rise due to piracy, conflict spillovers, or geopolitical tensions, the economic case for sustained security investment strengthens rather than weakens (One Earth Future Foundation, 2010; Mbekeani and Ncube, 2011). This formalizes the intuition from the international relations and defense economics literatures (Bueger et al., 2019; Kraska, 2015).

5.3 Structural Patterns

Network topology and vulnerability. The 78-node network reveals a structural distinction between two types of chokepoints. *Through-corridor chokepoints* (Malacca, Gibraltar, Suez, Bab el-Mandeb, Panama) connect large regions; their closure imposes rerouting costs on many port pairs but does not sever connectivity, because alternative maritime routes absorb rerouted traffic. *Bypass-dependent chokepoints* (Bosporus) are the primary connectors for ports behind them; their closure forces traffic onto expensive overland bypass routes. This distinction maps onto the theoretical framework of Fajgelbaum and Schaal (2020a), who show that optimal transport networks concentrate investment on high-throughput corridors.

Security priorities should therefore differ by chokepoint type. For through-corridor chokepoints, the objective is to minimize rerouting costs by maintaining capacity and reducing risk premiums. For bypass-dependent chokepoints, the objective is to prevent disruption that forces traffic onto dramatically more expensive alternatives. This connects to the congestion externality analysis of Hierons (2024): congestion pricing or capacity investment at through-corridor chokepoints can reduce rerouting costs, whereas bypass-dependent chokepoints require both security provision and investment in alternative infrastructure.

Nonlinear severity. The partial degradation analysis reveals that the relationship between disruption severity and cost increase is nonlinear. For through-corridor chokepoints,

severity curves accelerate at high degradation levels ($\alpha \geq 5$) as rerouting becomes the dominant response. Gibraltar and the Suez Canal exhibit the steepest severity curves, producing mean cost increases exceeding 26% and 12% respectively at $\alpha = 5$. This nonlinearity implies that the marginal return to reducing risk is highest at moderate disruption levels, suggesting that maintaining a credible deterrent captures most of the available dividend.

Heterogeneous vulnerability. The port vulnerability analysis reveals that the dividend is not uniformly distributed. Bypass-dependent ports (Black Sea) benefit most from their chokepoint’s security. Corridor-dependent ports (Mediterranean, South Asian, East African) benefit from the security of multiple chokepoints along their primary trade routes. Highly connected hub ports (Rotterdam, New York, Singapore) are relatively insulated. This heterogeneity implies that the political economy of maritime security investment is complex: the ports that benefit most from the public good are often in developing regions with limited capacity to contribute to its provision (Gaubert et al., 2025; Fajgelbaum et al., 2019). The geographic sorting dynamics studied by Desmet and Henderson (2015) and the agglomeration mechanisms of Duranton and Puga (2004) suggest that security investments may also affect the long-run spatial distribution of economic activity, as firms and workers adjust location decisions in response to changed trade-cost structures.

5.4 Limitations

We are explicit about several limitations that constrain interpretation while noting that each suggests a concrete direction for future work.

Static aggregate density. The AIS data aggregate vessel positions from January 2015 to February 2021 into a single snapshot. We cannot track temporal changes, seasonal variations, or dynamic adjustment to disruptions. Temporal disaggregation would enable analysis of how trade routes evolve in response to shocks (Cariou and Cheaitou, 2021; Du et al., 2020).

Aggregate density versus vessel-level flows. The density raster records total AIS positions without distinguishing vessel type, flag, cargo, or voyage. Extending to vessel-level AIS data would enable construction of origin-destination trade matrices and support estimation of the full spatial equilibrium model (Fajgelbaum and Schaal, 2020a; Allen and Arkolakis, 2022; Kerbl, 2022).

No welfare computation. Without bilateral trade volumes and demand elasticities, we cannot compute welfare changes in the general-equilibrium sense of Redding and Rossi-

Hansberg (2017) or Allen and Arkolakis (2025). Our delta-cost measures are informative about direction and relative magnitude but are not welfare estimates.

Exogenous security parameters. The security risk analysis treats risk premiums as exogenous inputs. In reality, security provision is endogenous to the strategic environment (Besley et al., 2015; Kraska, 2015). Endogenizing security would require a game-theoretic extension in which a security provider allocates resources across chokepoints to minimize expected trade-cost losses (Fajgelbaum and Gaubert, 2020).

5.5 Directions for Future Research

1. **Vessel-level AIS trajectories.** Individual vessel tracks would enable construction of origin-destination trade flow matrices and support estimation of route-choice models with probabilistic assignment (Fajgelbaum and Schaal, 2020a,b).
2. **Bilateral maritime trade data.** Combining vessel-level AIS with customs or port-authority trade data would enable calibration of a full spatial equilibrium model with endogenous demand (Redding and Rossi-Hansberg, 2017; Allen and Arkolakis, 2025; Redding, 2025).
3. **Insurance and risk pricing data.** War-risk insurance premiums and piracy incidence records would provide empirically grounded values for the security parameters (Besley et al., 2015; One Earth Future Foundation, 2010).
4. **Naval presence proxies.** Open-source data on naval deployments would enable causal estimation of the security provision effect.
5. **Dynamic extensions.** A time-varying network with stochastic disruptions and adjustment costs would capture the temporal dimension of chokepoint risk (Hierons, 2024; Bordeu, 2025).
6. **Optimal security allocation.** A normative extension could solve for the optimal spatial allocation of security resources, building on Rossi-Hansberg (2004), Fajgelbaum and Gaubert (2020, 2025), and Gaubert et al. (2025): given a fixed security budget, which chokepoints should receive the most protection?
7. **Political economy of burden-sharing.** The observation that maritime security is a global public good with concentrated provision raises questions about sustainability and equity. An extension incorporating political-economy considerations (Fajgelbaum et al., 2019; Bordeu, 2025) could analyze the efficiency and distributional consequences of alternative burden-sharing regimes. The frameworks of Owens et al. (2020) and Rossi-Hansberg et al. (2023) offer tools for evaluating how spatial redistribution interacts with agglomeration and connectivity.

6 Conclusion

Maritime security is a global public good whose economic value has been under-studied relative to its importance. This paper contributes a transparent, replicable framework for measuring chokepoint vulnerability and quantifying the hegemonic dividend from security provision. Using AIS density data from the IMF, we constructed a 78-node maritime transport network with 1,540 port-to-port trade routes and implemented a multi-scenario stress-testing engine.

Three main findings emerge. First, chokepoint disruptions produce large and heterogeneous trade-cost increases: the Panama Canal (mean rerouting cost of 17,840 km-equivalent), Gibraltar (10,624 km), and the Suez Canal (9,949 km) generate the largest rerouting costs when fully closed, while the bypass-dependent Bosphorus forces Black Sea ports onto an expensive overland alternative at $5\times$ normal maritime cost. Second, the marginal value of security provision is increasing in the risk environment: the hegemonic dividend is largest precisely when security conditions are deteriorating. Third, the vulnerability is highly heterogeneous across ports, with bypass-dependent and corridor-dependent developing-region ports benefiting most from the global public good of maritime security. Our cost-per-day estimates—ranging from \$16 million to \$233 million per day depending on the chokepoint—provide a concrete, policy-relevant metric for evaluating the economic value of maritime security provision.

These findings are offered as a data-grounded first step that identifies the data requirements and modeling extensions needed for a full causal assessment. The orders of magnitude—rerouting costs translating to tens of billions of dollars annually, with the most affected port pairs facing cost increases of 10,000–18,000 km-equivalent—suggest that the economic stakes of maritime security provision are substantial, and that the hegemonic dividend from concentrated security at critical chokepoints is a first-order feature of the global trading system.

References

- Allen, T. and Arkolakis, C. (2022). The welfare effects of transportation infrastructure improvements. *Review of Economic Studies*, 89(6):2911–2957.
- Allen, T. and Arkolakis, C. (2025). Quantitative regional economics. In *Handbook of Urban and Regional Economics*, volume 6, chapter 1. Elsevier.
- Besley, T., Fetzer, T., and Mueller, H. (2015). The welfare cost of lawlessness: Evidence from Somali piracy. *Journal of the European Economic Association*, 13(6):979–997.
- Bordeu, O. (2025). Commuting infrastructure in fragmented cities. Working Paper.
- Bueger, C., Edmunds, T., and Ryan, B. J. (2019). Maritime security: The uncharted politics of the global sea. *International Affairs*, 95(5):971–978.
- Bueger, C., Edmunds, T. P., and Stockbruegger, J. (2024). Securing the seas: A comprehensive assessment of global maritime security. Technical report, SafeSeas.
- Cariou, P. and Cheaitou, A. (2021). The use of AIS data to analyse the economic impact of disruptive events on container flows and ship waiting times in main ports. *Maritime Economics & Logistics*, 23(4):605–625.
- Cerdeiro, D. A. and Komaromi, A. (2020). Nowcasting world trade using AIS data: A machine learning approach. *IMF Working Paper*, (WP/20/90).
- Cerdeiro, D. A., Komaromi, A., Liu, Y., and Saeed, M. (2020). World seaborne trade in real time: A proof of concept for building AIS-based nowcasts from scratch. IMF Working Paper WP/20/57, International Monetary Fund.
- Desmet, K. and Henderson, J. V. (2015). The geography of development within countries. In *Handbook of Regional and Urban Economics*, volume 5, chapter 22. Elsevier.
- Donaldson, D. (2025). Transport infrastructure and policy evaluation. In *Handbook of Regional and Urban Economics*, volume 6, chapter 5, pages 287–352. Elsevier.
- Du, Y., Wang, S., and Meng, Q. (2020). How are ports tackling congestion and delays? *Maritime Policy & Management*, 47(5):603–617.
- Duranton, G. and Puga, D. (2004). Micro-foundations of urban agglomeration economies. In *Handbook of Regional and Urban Economics*, volume 4, chapter 48. Elsevier.

- Fajgelbaum, P. D. and Gaubert, C. (2020). Optimal spatial policies, geography, and sorting. *Quarterly Journal of Economics*, 135(2):959–1036.
- Fajgelbaum, P. D. and Gaubert, C. (2025). Optimal spatial policies. In *Handbook of Urban and Regional Economics*, volume 6, chapter 3. Elsevier.
- Fajgelbaum, P. D., Morales, E., Suárez Serrato, J. C., and Zidar, O. (2019). State taxes and spatial misallocation. *Review of Economic Studies*, 86(1):333–376.
- Fajgelbaum, P. D. and Schaal, E. (2020a). Optimal transport networks in spatial equilibrium. *Econometrica*, 88(4):1411–1452.
- Fajgelbaum, P. D. and Schaal, E. (2020b). Supplement to “Optimal Transport Networks in Spatial Equilibrium”. *Econometrica Supplementary Material*, 88(4).
- Gaubert, C., Kline, P., and Yagan, D. (2025). Place-based redistribution. Working Paper.
- Hierons, T. (2024). Spreading the jam: Optimal congestion pricing in general equilibrium. Working Paper.
- Kerbl, S. (2022). Economic research with AIS data. *CESifo Forum*, 23(1):43–47.
- Kraska, J. (2015). Law of the sea. In *The Oxford Handbook of the Use of Force in International Law*. Oxford University Press.
- Mbekeani, K. K. and Ncube, M. (2011). Economic impact of maritime piracy. Africa Economic Brief 10, African Development Bank.
- Morabito, G. (2023). *Maritime Transport Economics and Policy*. PhD thesis, University of Messina.
- Notteboom, T. E. (2006). The impact of port congestion on freight rates and the shipping industry. *Journal of Transport Geography*, 14(3):197–212.
- One Earth Future Foundation (2010). The economic cost of piracy. Technical report, Oceans Beyond Piracy.
- Owens, R., Rossi-Hansberg, E., and Sarte, P.-D. (2020). Rethinking Detroit. *American Economic Journal: Economic Policy*, 12(2):258–305.
- Proost, S. and Thisse, J.-F. (2019). What can be learned from spatial economics? *Journal of Economic Literature*, 57(3):575–643.

- Redding, S. J. (2025). Quantitative urban economics. In *Handbook of Urban and Regional Economics*, volume 6, chapter 2. Elsevier.
- Redding, S. J. and Rossi-Hansberg, E. (2017). Quantitative spatial economics. *Annual Review of Economics*, 9:21–58.
- Rossi-Hansberg, E. (2004). Optimal urban land use and zoning. *Review of Economic Dynamics*, 7(1):69–106.
- Rossi-Hansberg, E. (2020). Transportation networks. Lecture slides, University of Chicago.
- Rossi-Hansberg, E., Sarte, P.-D., and Schwartzman, F. (2023). Cognitive hubs and spatial redistribution. *American Economic Journal: Macroeconomics*, 15(3):254–299.
- Verschuur, J., Lumma, J., and Hall, J. W. (2023). Systemic impacts of disruptions at maritime chokepoints. *Nature Communications*, 14(1):5945.

A Cost and Distance Assumptions

Our scenario engine reports rerouting costs in *km-equivalent* units, reflecting weighted shortest-path distances through the maritime network. To translate these into approximate economic magnitudes, Table 4 documents all assumptions used in the cost mapping.

Table 4: Cost and Distance Assumptions

Parameter	Value	Units	Justification & Source
Haversine distance	dis-	Computed km	Great-circle distance between node coordinates; standard geodesic formula (Allen and Arkolakis, 2022)
Congestion multiplier range	[1.0, 1.5]	dimensionless	Calibrated from AIS density via log-linear mapping; upper bound consistent with port congestion estimates (Nottet-boom, 2006)

Continued on next page

Parameter	Value	Units	Justification & Source
Overland by-pass: Bosphorus (Constanta–Piraeus)	$5.0 \times$ haver-sine	km-equiv.	Rail/truck intermodal alternative through southeastern Europe; overland freight typically $3\text{--}6 \times$ maritime cost (Notteboom, 2006)
Fuel cost (bunker)	\$400–600	per tonne	IFO 380 benchmark price range 2019–2023; IMO 2020 sulphur cap increased costs by 25–40% for compliant fuels (Notteboom, 2006)
Average fuel consumption	150–250	tonnes/day	Typical for Panamax–post-Panamax container vessels at design speed (Du et al., 2020)
Shipping cost per tonne-km	\$5–10	per 1,000 km	Containerized cargo; range reflects vessel size, fuel prices, and route (Notteboom, 2006)
War-risk insurance premium	0.1–0.5%	of hull value	Baseline range; can spike to 1–5% in conflict zones (Besley et al., 2015 ; One Earth Future Foundation, 2010)
Canal transit tolls: Suez	\$0.3–1.0M	per transit	Varies by vessel size and cargo type; represents 2–8% of total voyage cost for Asia–Europe routes (Cariou and Cheaitou, 2021)
Canal transit tolls: Panama	\$0.2–0.8M	per transit	New Panamax locks increased capacity but raised tolls (Notteboom, 2006)
Average vessel speed	12–16	knots	Slow-steaming range for fuel efficiency (Du et al., 2020)
Daily time charter rate	\$10,000–50,000	per day	Container vessel range depending on size and market conditions (Notteboom, 2006)

Continued on next page

Parameter	Value	Units	Justification & Source
Crew cost	\$3,000–8,000	per day	All-in crew cost for 20–25 person complement (One Earth Future Foundation, 2010)
Risk premium scenarios	10–200%	of base cost	Applied to chokepoint-adjacent edges; upper range consistent with war-risk premium spikes observed during Gulf conflicts (Besley et al., 2015)
Partial degradation multiplier	1.25–10×	dimensionless	Range captures mild congestion (1.25×) through near-closure (10×)
Global seaborne trade volume	~11 billion tonnes/year	UNCTAD 2023 estimate; used for order-of-magnitude cost translations (Verschuur et al., 2023)	

Translating km-equivalent to economic costs. A mean rerouting cost of Δ km-equivalent can be approximately converted to annual economic impact as:

$$\text{Annual cost} \approx \Delta \times \frac{\text{Trade volume (tonnes)}}{\text{Average voyage distance}} \times \text{Cost per tonne-km}, \quad (9)$$

where we use illustrative values of \$5–10 per tonne per 1,000 km for containerized cargo and approximately 11 billion tonnes of global seaborne trade. These conversions are intended as order-of-magnitude estimates; precise economic costs depend on cargo composition, vessel types, demand elasticities, and market conditions that are beyond the scope of this analysis.

Sensitivity analysis. We conduct sensitivity analysis along three dimensions: (i) bounding box size (expanding/contracting chokepoint definitions by 20%); (ii) congestion parameter (λ varied from 0 to 0.3); and (iii) cost multiplier range for the congestion normalization. These checks ensure that results are not artifacts of arbitrary parameter choices.

B Chokepoint Bounding Box Maps

Figure 19 shows all six chokepoint bounding boxes on a single world map. Figures 20–25 show individual zoomed maps for each chokepoint, with the AIS density visible in the background and the bounding box coordinates annotated.

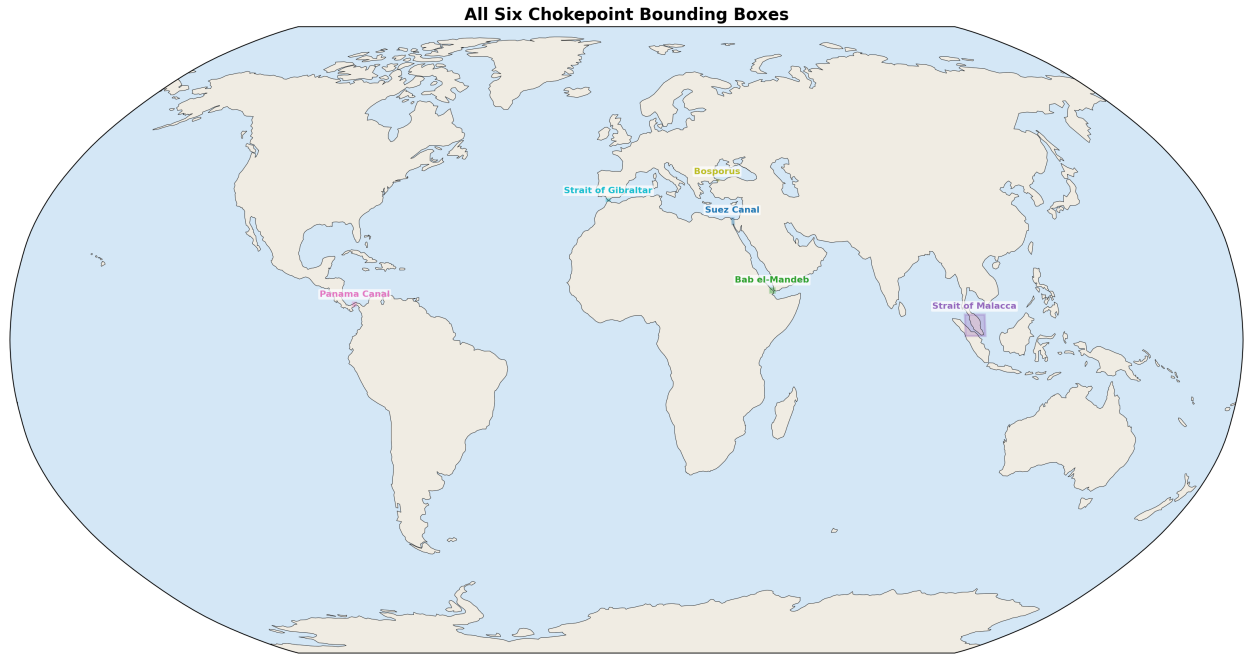


Figure 19: All six chokepoint bounding boxes overlaid on a world map.

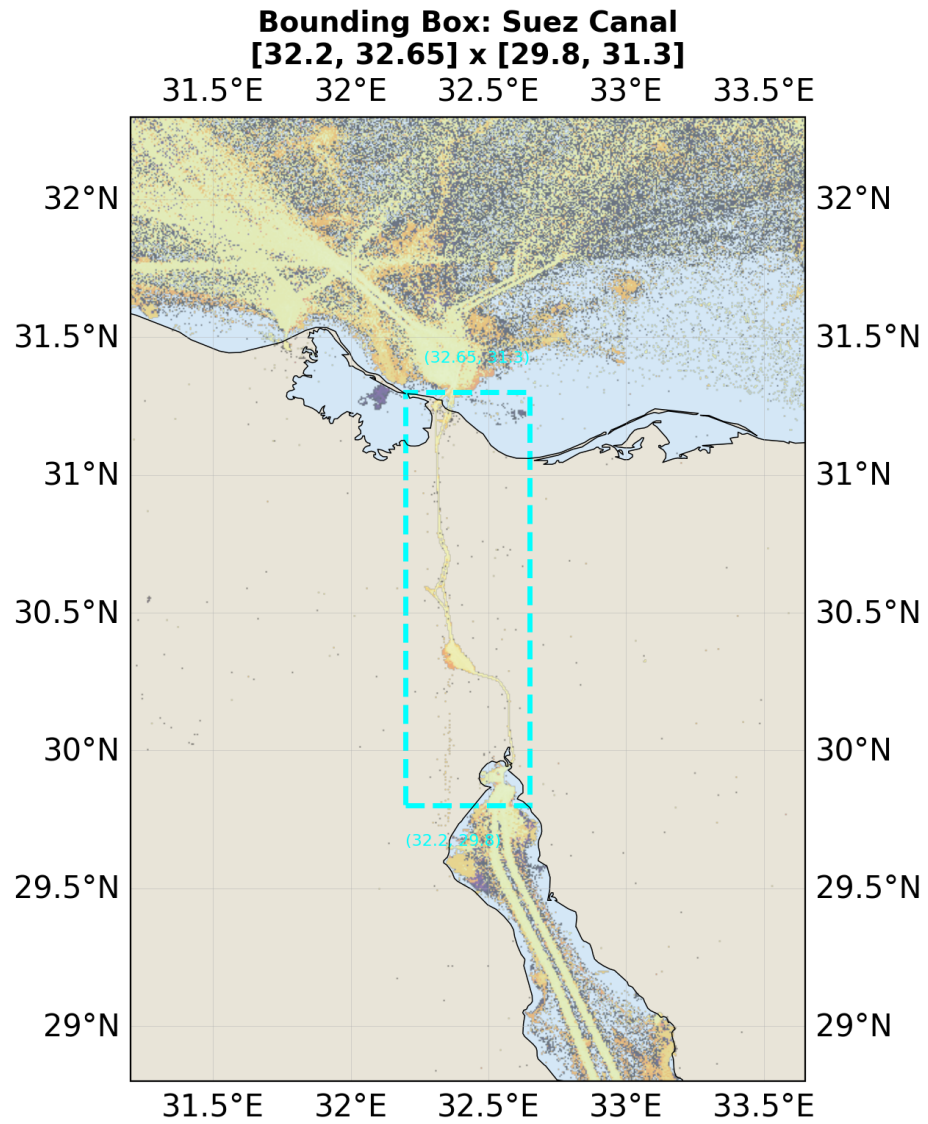


Figure 20: Bounding box: Suez Canal.

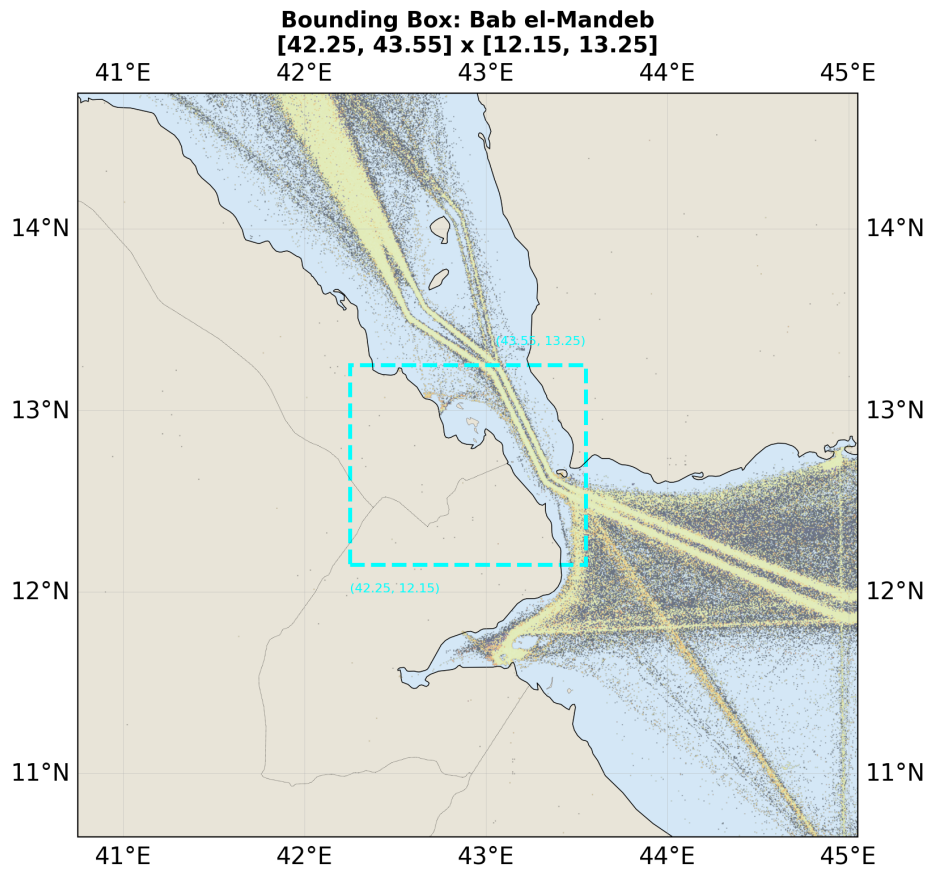


Figure 21: Bounding box: Bab el-Mandeb.

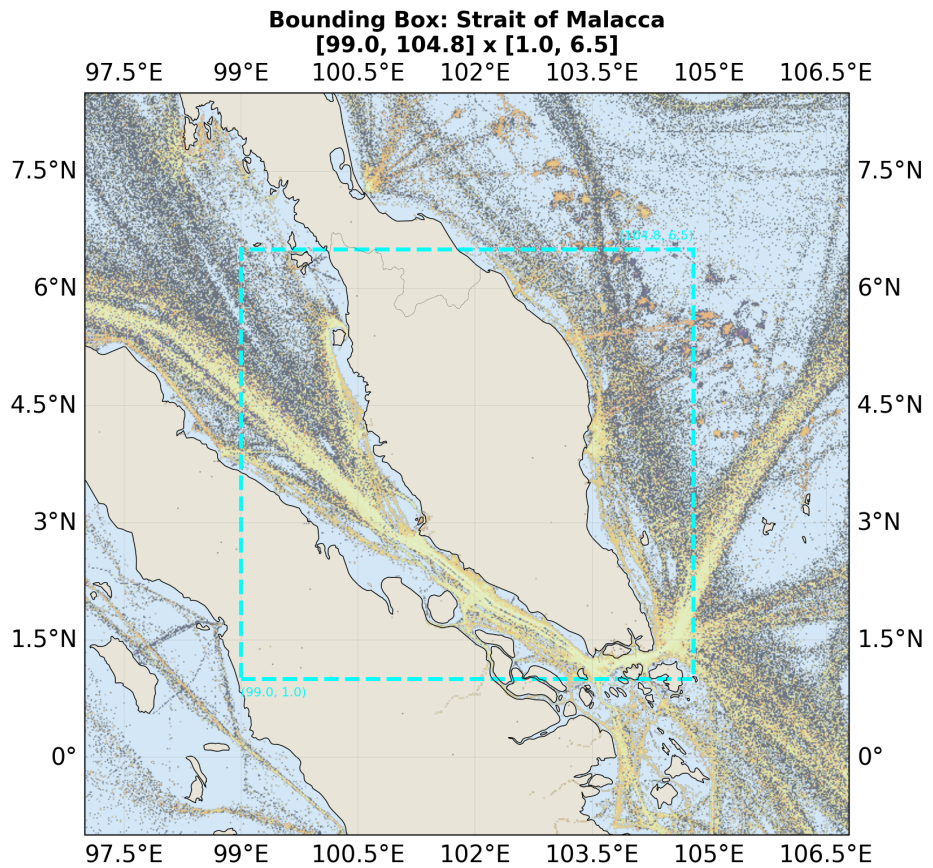


Figure 22: Bounding box: Strait of Malacca.

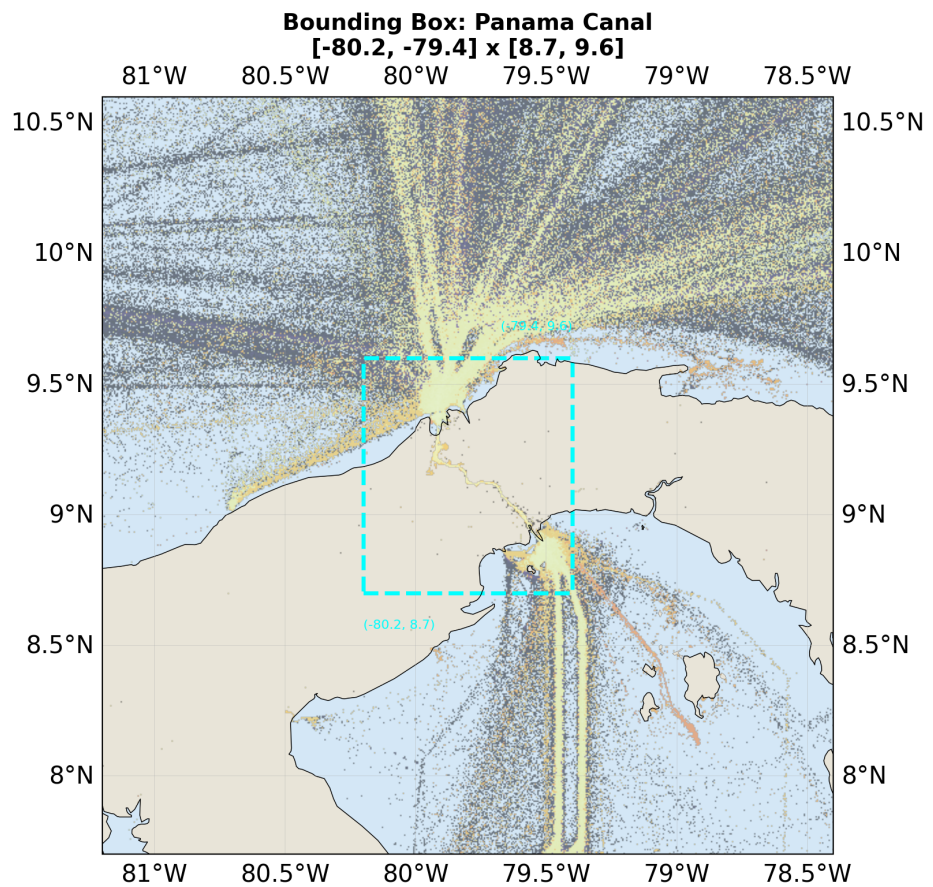


Figure 23: Bounding box: Panama Canal.

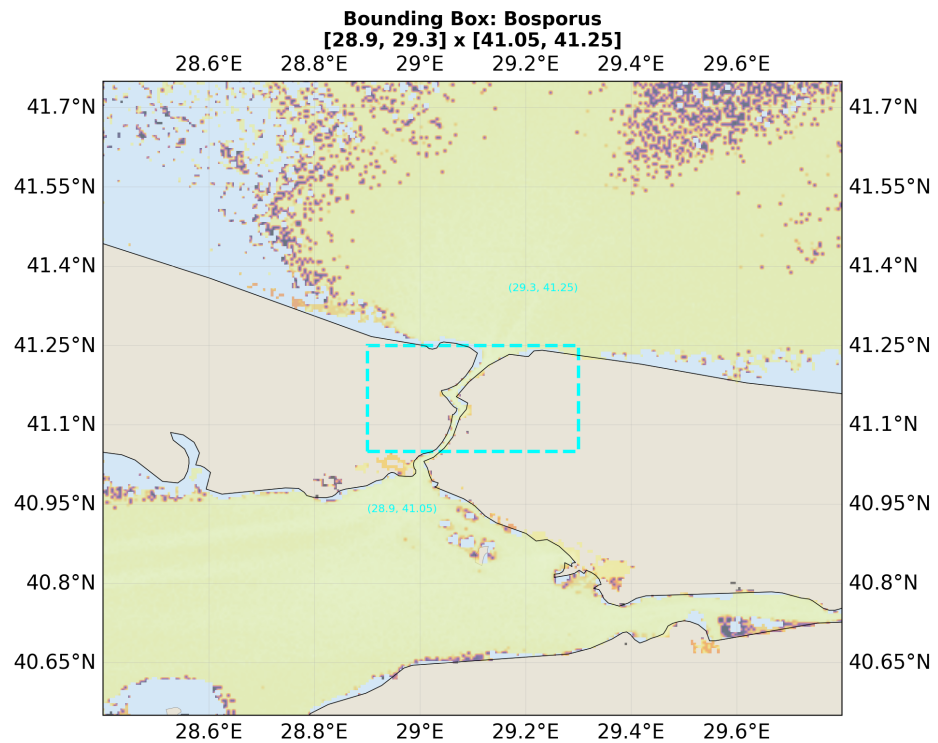


Figure 24: Bounding box: Bosphorus.

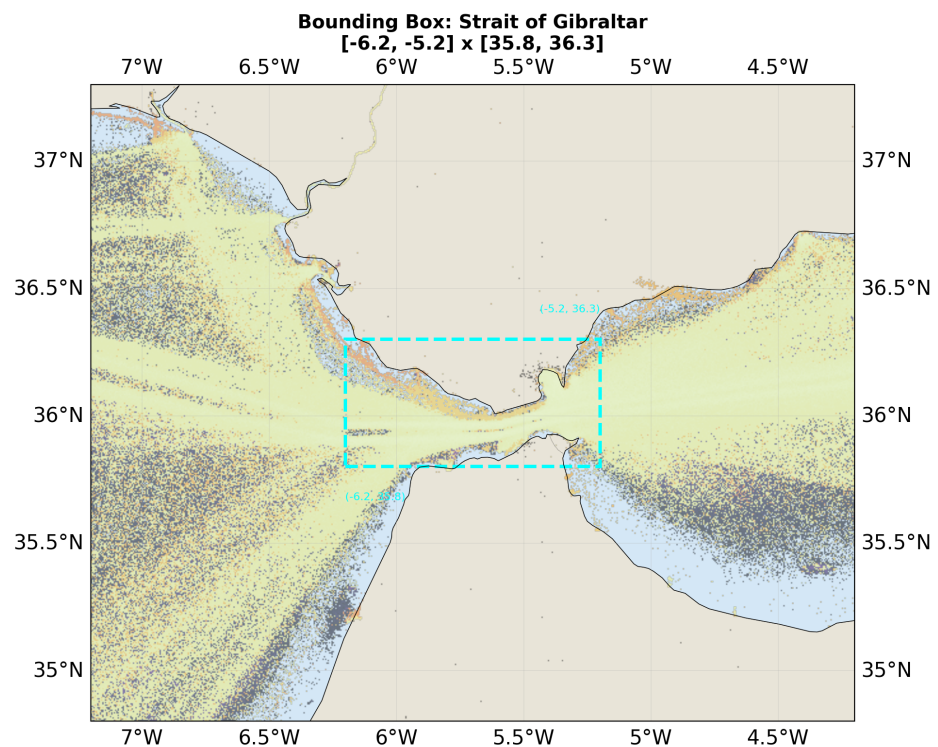


Figure 25: Bounding box: Strait of Gibraltar.

C Chokepoint Traffic Density Close-ups

Figures 26–31 show zoomed AIS density overlays for each chokepoint bounding box, with intensity statistics annotated.

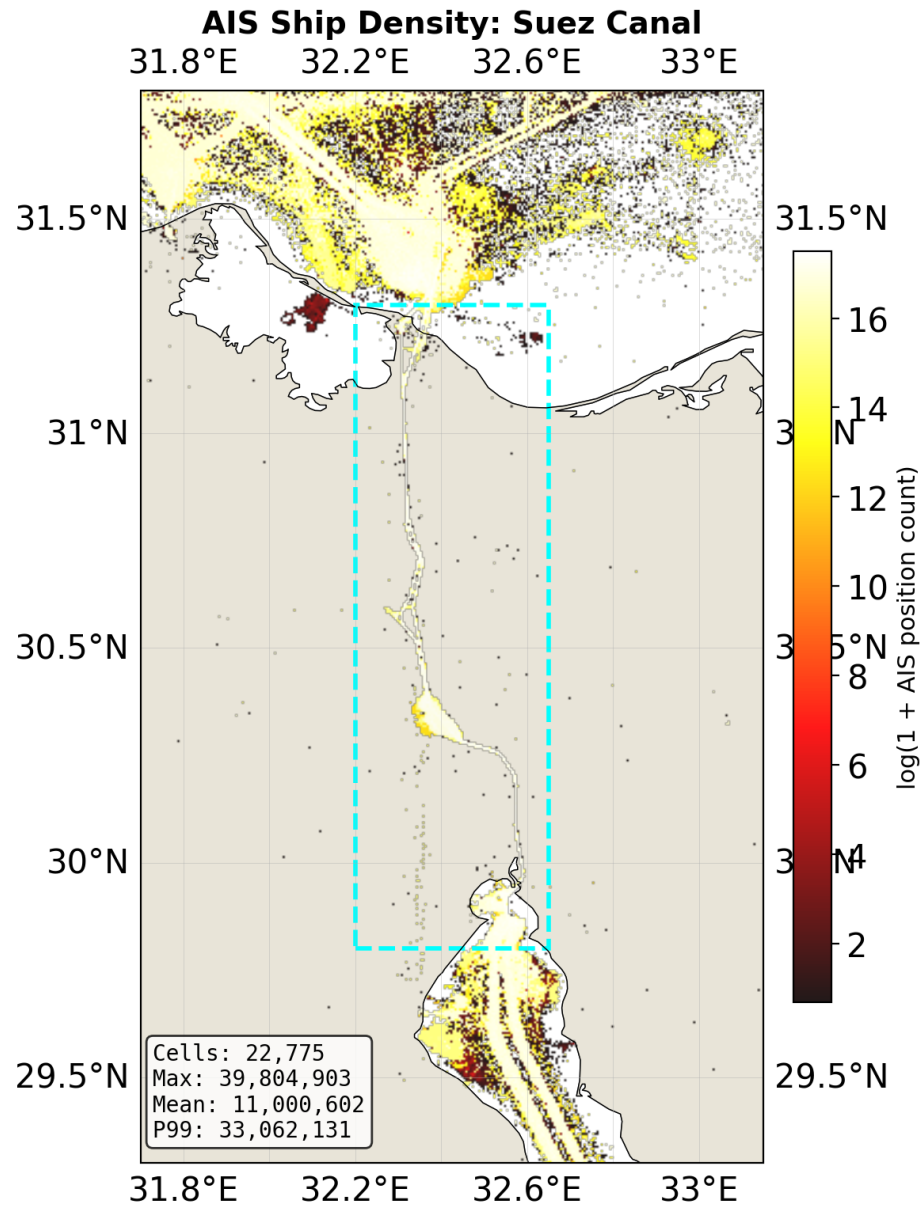


Figure 26: AIS density: Suez Canal.

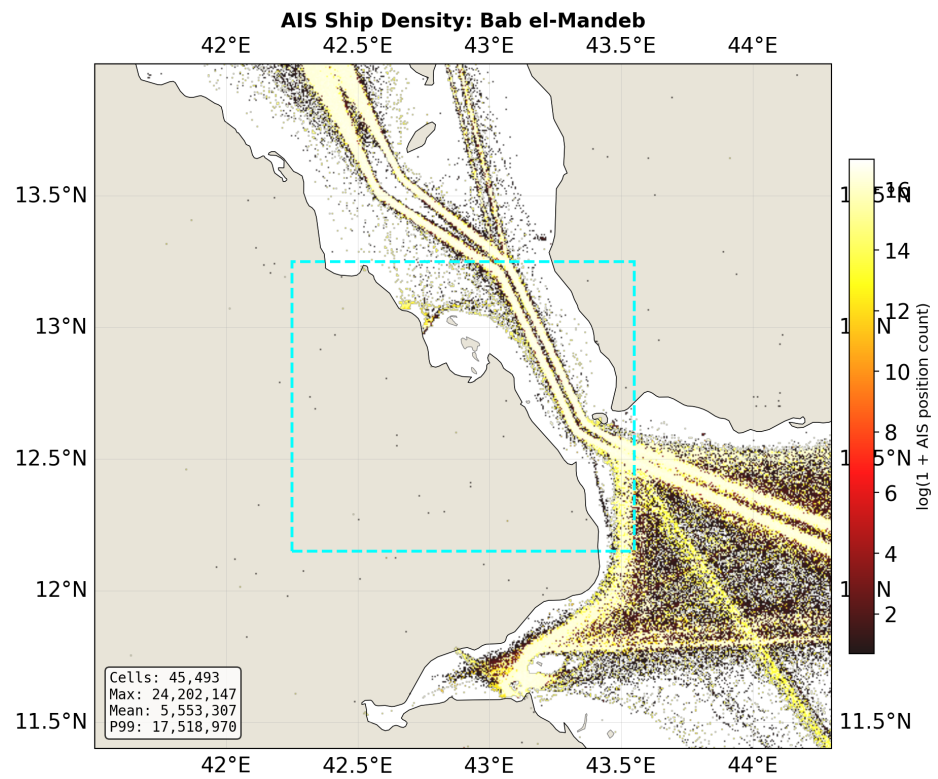


Figure 27: AIS density: Bab el-Mandeb.

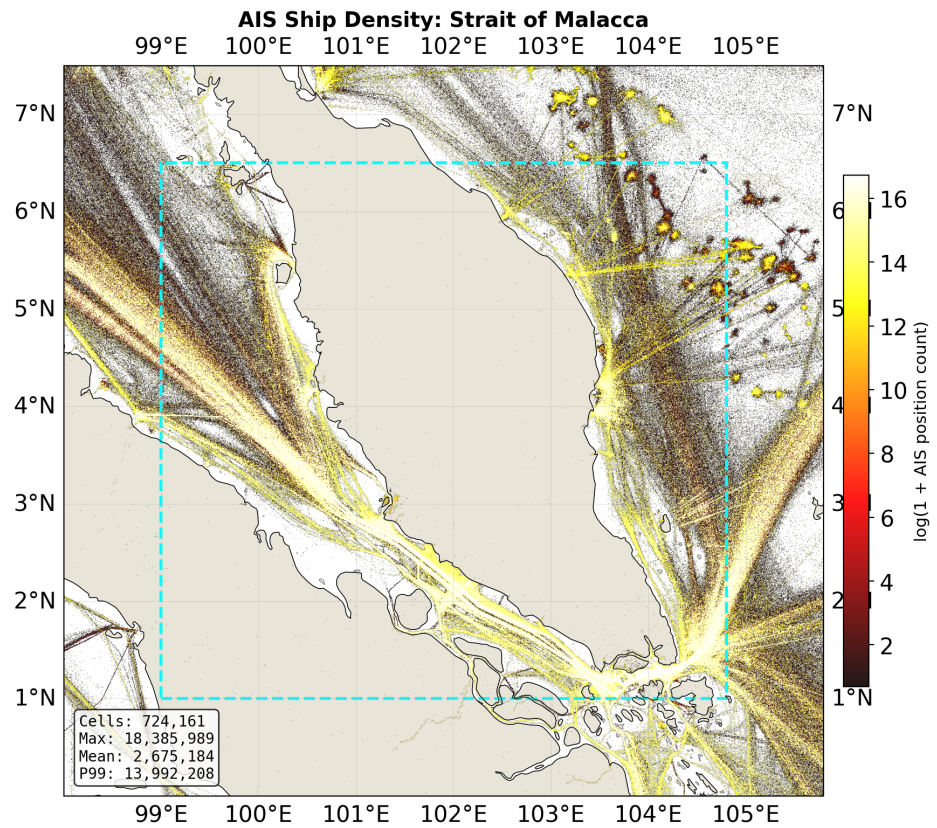


Figure 28: AIS density: Strait of Malacca.

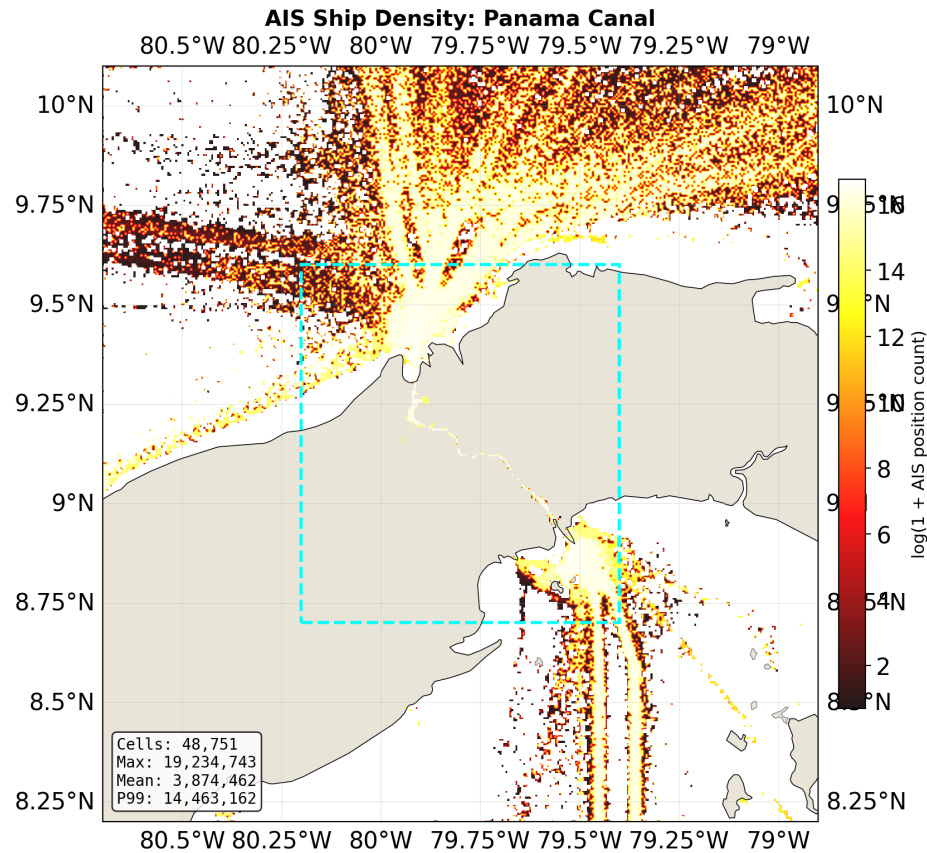


Figure 29: AIS density: Panama Canal.

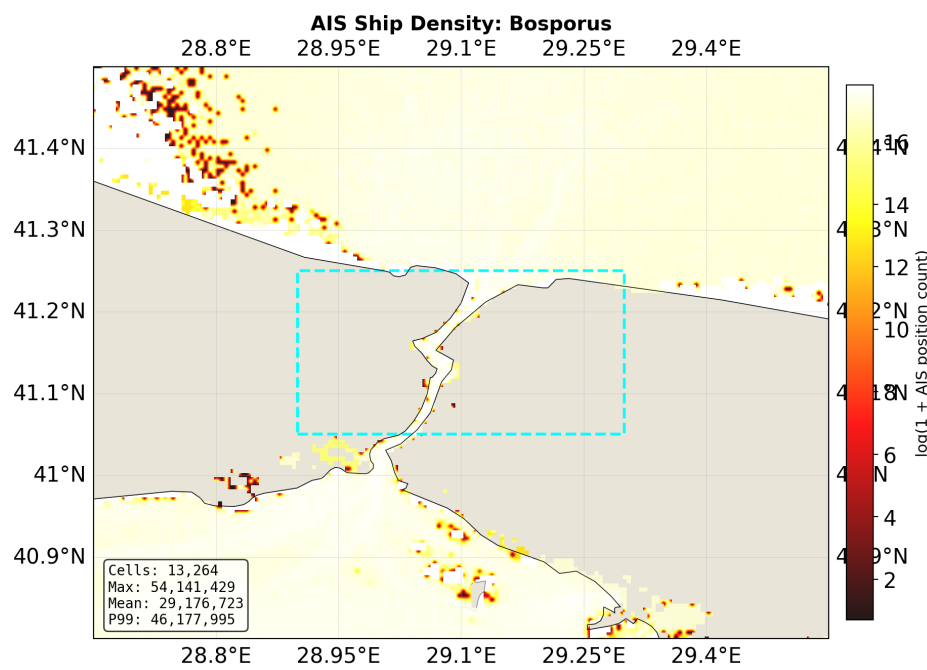


Figure 30: AIS density: Bosphorus.

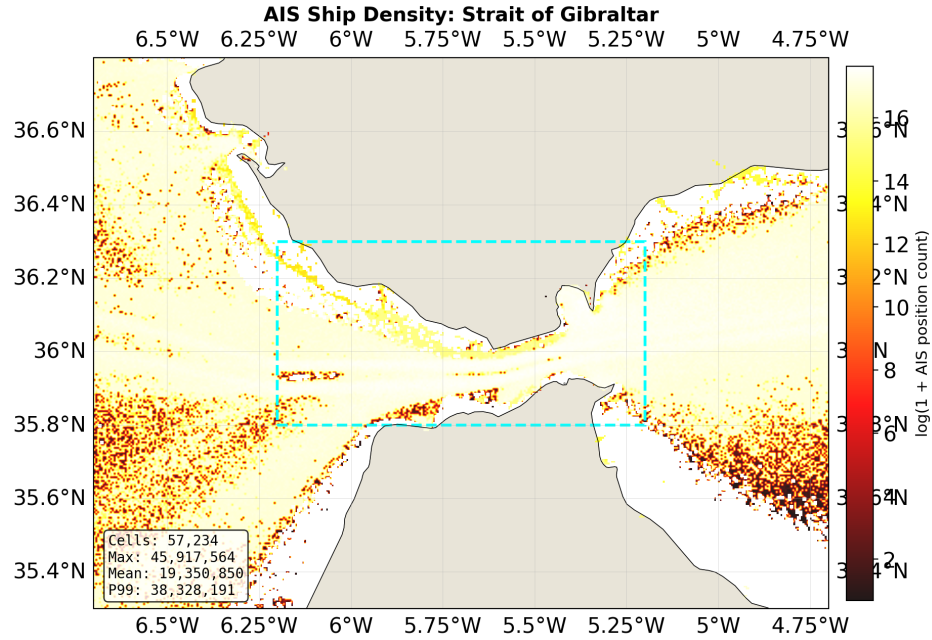


Figure 31: AIS density: Strait of Gibraltar.

D Chokepoint Descriptive Statistics

The full chokepoint intensity table is reported below, followed by descriptive statistics figures for each chokepoint.

Table 5: Chokepoint traffic intensity from AIS raster data. Sum intensity reflects total vessel traffic density within each chokepoint bounding box.

Chokepoint	Sum Intensity	Mean Intensity	P99 Cell	Grid Cells	Rank
Strait of Malacca	1.21T	945.8K	12.61M	1,276,000	1
Gibraltar	249.01B	12.45M	40.31M	20,000	2
Bab el Mandeb	46.04B	804.9K	15.90M	57,200	3
Panama Canal	40.36B	1.40M	15.39M	28,800	4
Suez Canal	35.79B	1.33M	32.09M	27,000	5
Bosporus	11.36B	3.55M	48.42M	3,200	6

Chokepoint Analysis: Suez Canal

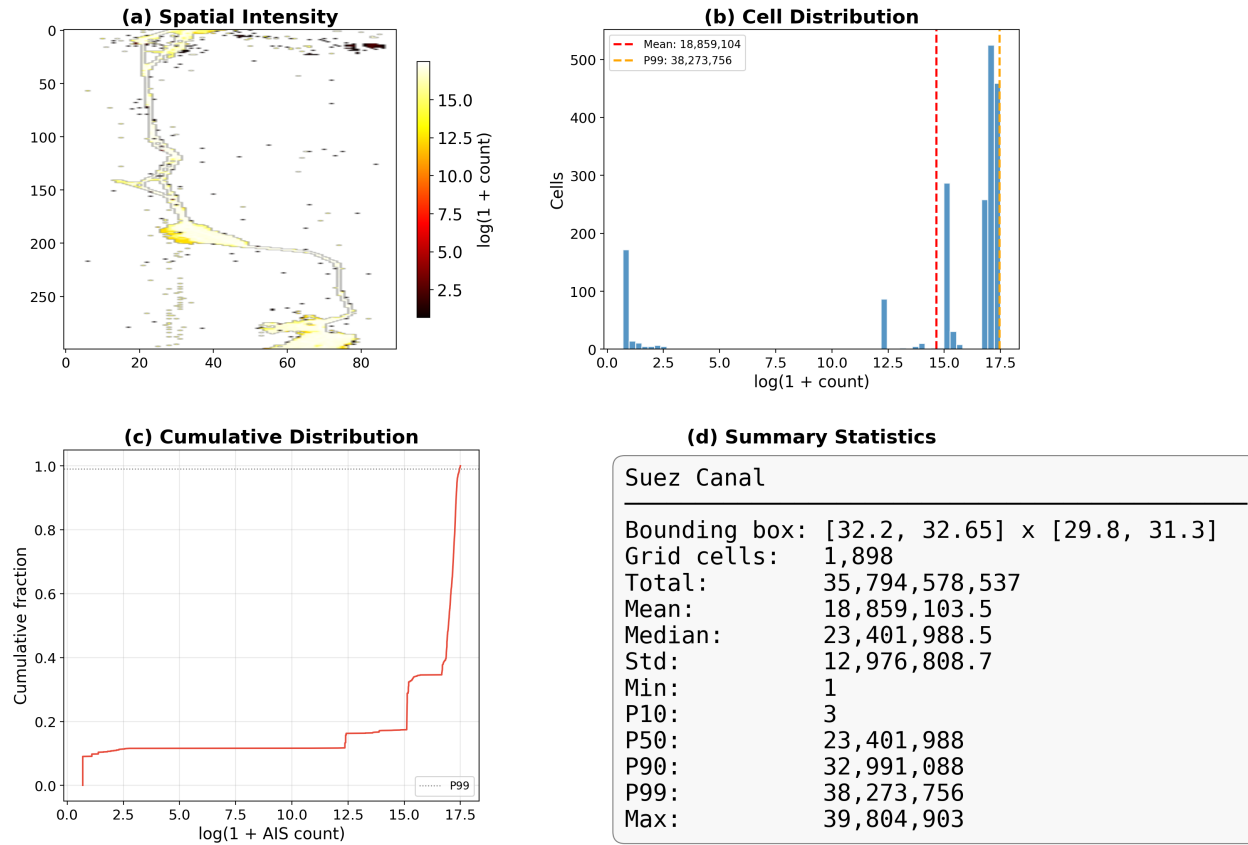


Figure 32: Descriptive statistics: Suez Canal.

Chokepoint Analysis: Bab el-Mandeb

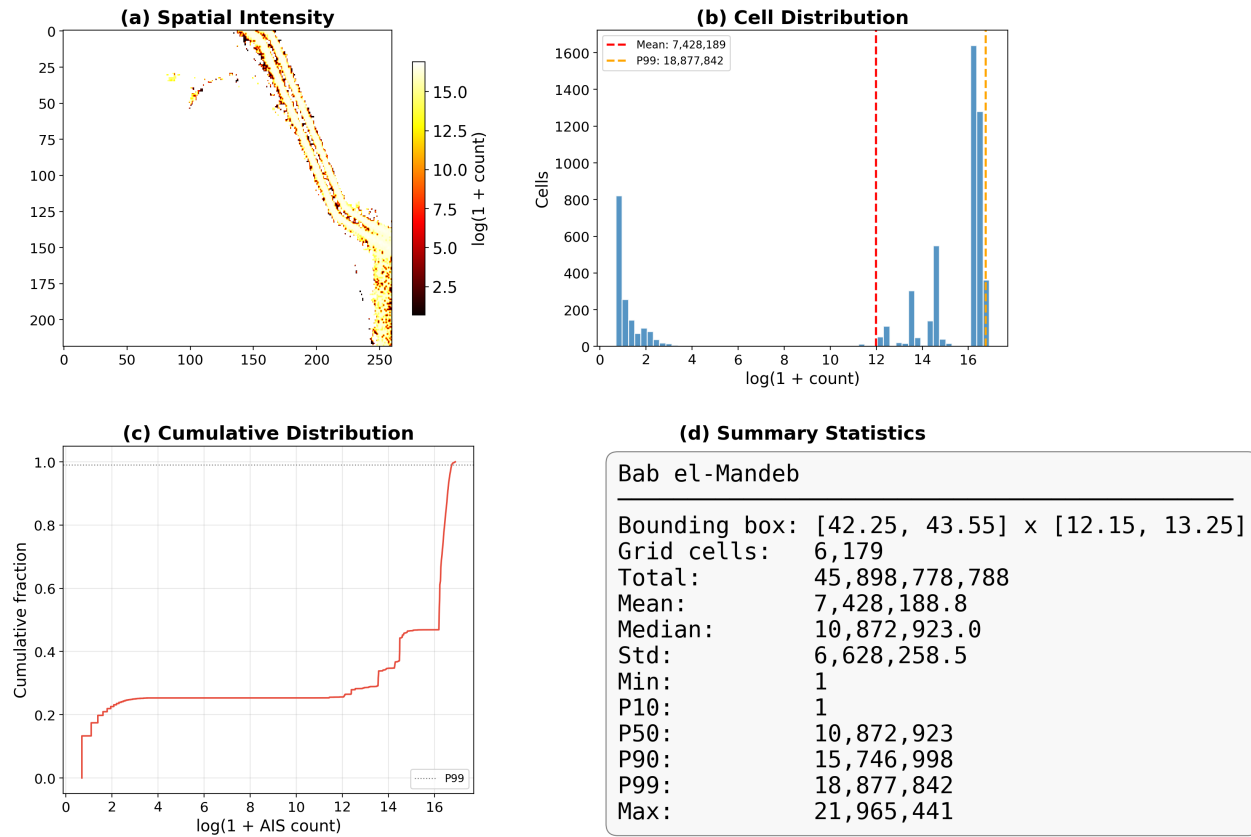


Figure 33: Descriptive statistics: Bab el-Mandeb.

Chokepoint Analysis: Strait of Malacca

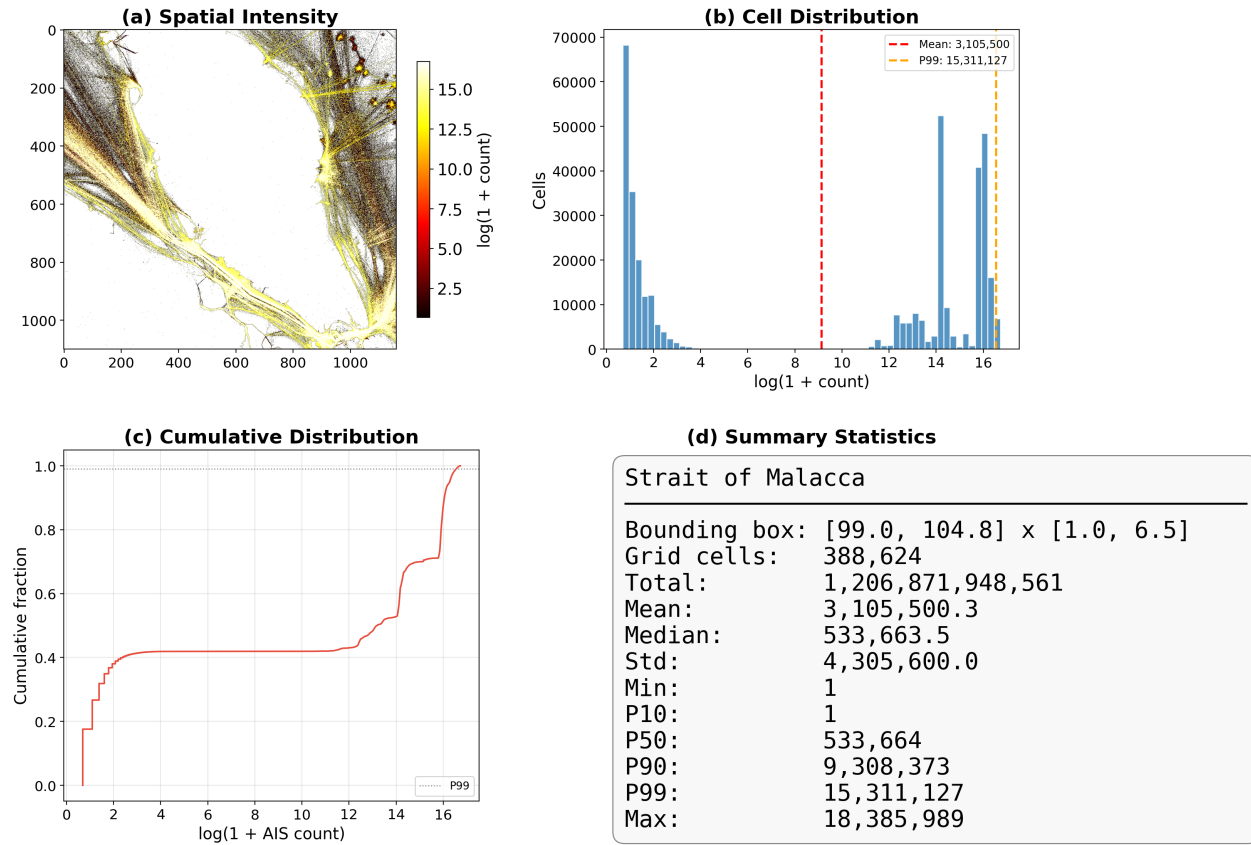


Figure 34: Descriptive statistics: Strait of Malacca.

Chokepoint Analysis: Panama Canal

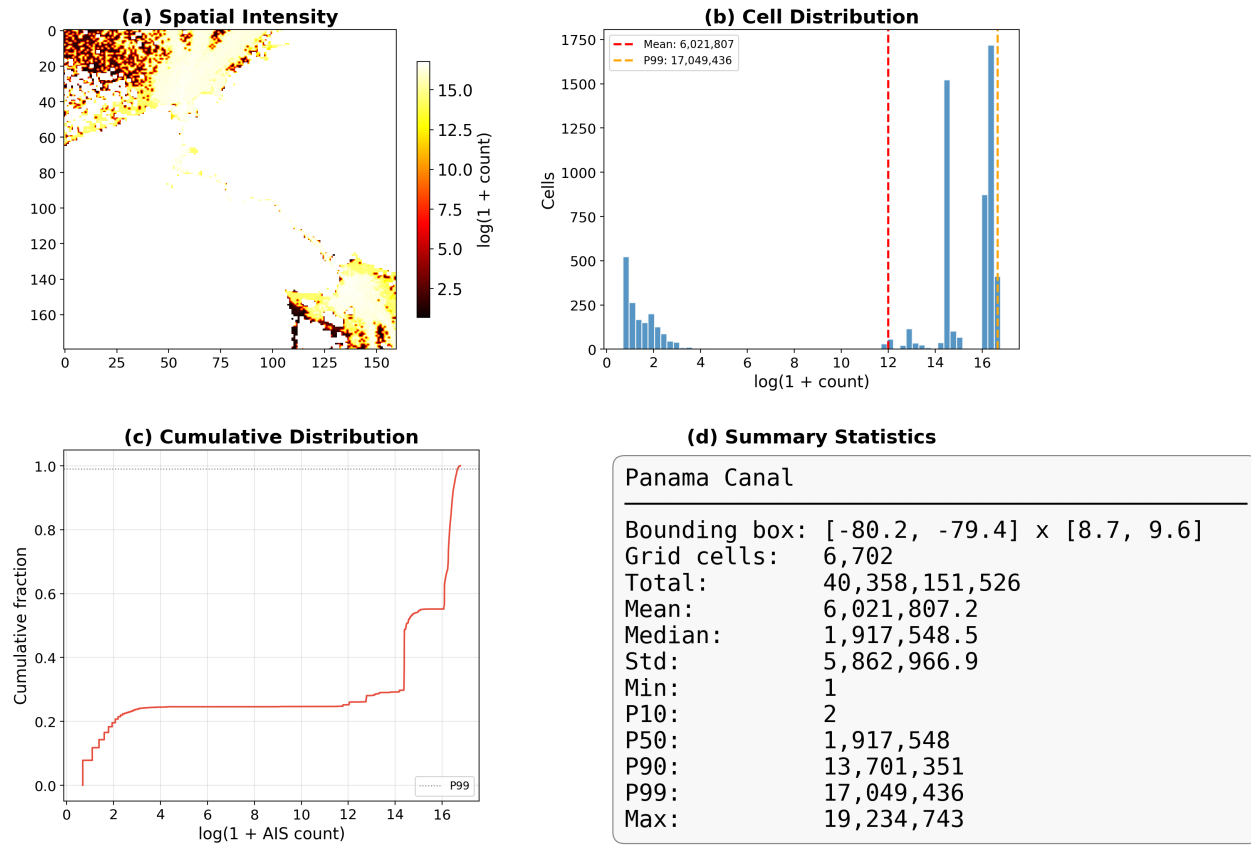


Figure 35: Descriptive statistics: Panama Canal.

Chokepoint Analysis: Bosphorus

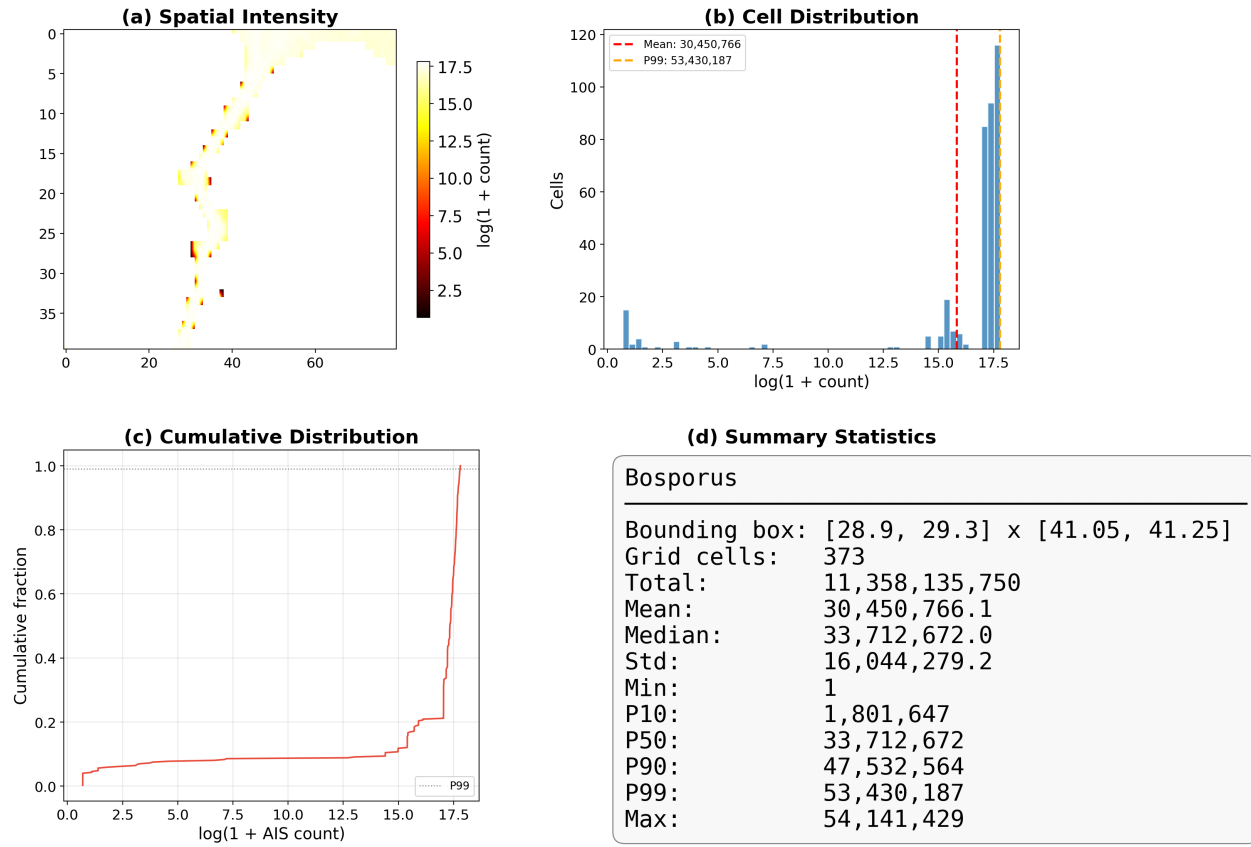


Figure 36: Descriptive statistics: Bosphorus.

Chokepoint Analysis: Strait of Gibraltar

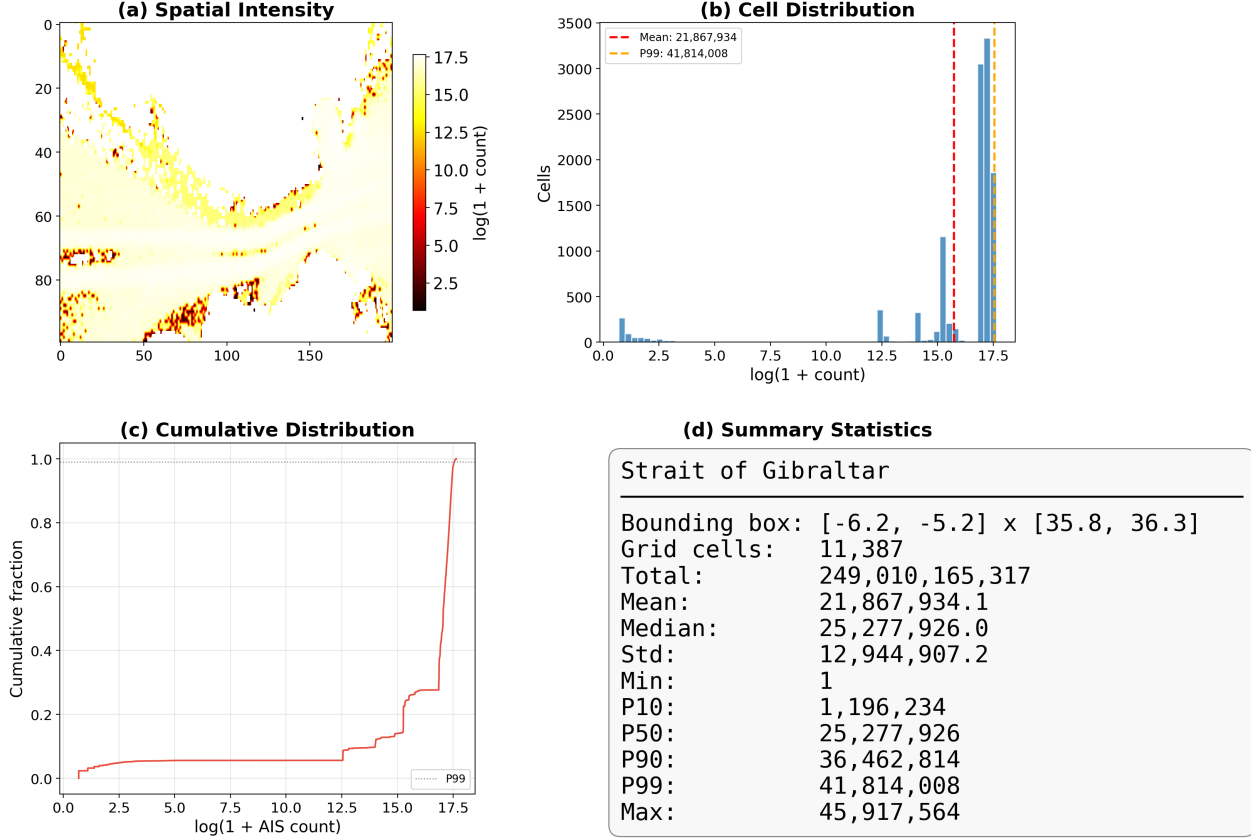


Figure 37: Descriptive statistics: Strait of Gibraltar.

E Ship-Count Estimation Under Closure Scenarios

E.1 Baseline Annual Transit Estimates

To translate our network-based rerouting costs into concrete operational magnitudes, we estimate the number of vessels affected by each chokepoint closure scenario. We draw baseline annual transit counts from published sources—canal authority statistics, UNCTAD reports, and U.S. Energy Information Administration (EIA) data—rather than attempting to reverse-engineer vessel counts from our aggregate AIS density raster, which records cumulative position reports without distinguishing individual vessel transits.

Table 6 reports the baseline annual transit estimates for each chokepoint, along with the data source and the approximate range reflecting inter-year variation over the 2015–2021 period.

Table 6: Estimated annual vessel transits at each chokepoint. Ranges reflect inter-year variation over 2015–2021 and rounding uncertainty.

Chokepoint	Central Estimate	Range	Source
Strait of Gibraltar	80,000	70,000–100,000	UNCTAD, Verschuur et al. (2023)
Strait of Malacca	85,000	80,000–94,000	IMO, UNCTAD
Bosporus	43,000	40,000–46,000	Turkish Directorate General
Bab el-Mandeb	25,000	20,000–30,000	UNCTAD, EIA
Suez Canal	19,500	18,000–20,700	Suez Canal Authority
Panama Canal	13,500	12,000–14,500	Panama Canal Authority

Several caveats apply to these estimates. First, “transits” count individual vessel passages through the chokepoint; a vessel that makes multiple round trips during a year is counted multiple times. Second, transit counts include all vessel types (container ships, tankers, bulk carriers, military vessels, fishing vessels, passenger ships), not only cargo-carrying vessels relevant to trade. Third, the AIS density data in our primary analysis include vessel *positions* (typically broadcast every 2–10 seconds), which are far more numerous than vessel transits. The distinction between cumulative AIS position counts and discrete vessel transits is critical: a single vessel transiting a chokepoint bounding box generates thousands to tens of thousands of AIS position reports depending on the transit duration and broadcast frequency.

E.2 Vessels Affected by Closure Scenarios

We estimate the number of vessels affected by each closure scenario by combining the baseline transit counts with the fraction of port pairs affected from our full closure analysis (Section 4.3). For each chokepoint b , the fraction of port pairs affected is $f_b = \text{Pairs Affected}_b / 1,540$. We multiply this fraction by the annual transit count to produce an *order-of-magnitude* estimate of vessels requiring rerouting.

This approach rests on two simplifying assumptions that we state explicitly:

1. **Uniform traffic distribution:** We assume that vessel transits are approximately uniformly distributed across port pairs that use the chokepoint. In reality, a small number of high-volume trade corridors (e.g., Asia–Europe via Suez) dominate transit counts, so the actual number of affected vessels could be higher or lower than our estimate depending on whether high-volume pairs are disproportionately affected.
2. **Transit–pair proportionality:** We assume that the fraction of transits affected is proportional to the fraction of port pairs affected. This would be exact if all port pairs

generated equal traffic volumes, which is clearly not the case. We therefore report our estimates as order-of-magnitude bounds.

Table 7 reports the estimated vessels affected under each full closure scenario.

Table 7: Estimated annual vessels affected by chokepoint closure. Lower and upper bounds reflect the uncertainty range in baseline transit counts. “Rerouted” vessels must find alternative maritime routes; no vessels are fully disconnected under our network design (bypass routes exist for all chokepoints).

Chokepoint Closed	Pairs Affected (%)	Central Est.	Lower Bound	Upper Bound
Panama Canal	298 (19.4%)	2,600	2,300	2,800
Gibraltar	590 (38.3%)	30,600	26,800	38,300
Suez Canal	469 (30.5%)	5,900	5,500	6,300
Bab el-Mandeb	454 (29.5%)	7,400	5,900	8,800
Bosporus	159 (10.3%)	4,400	4,100	4,700
Strait of Malacca	290 (18.8%)	16,000	15,100	17,700

E.3 Interpretation and Uncertainty

The estimates in Table 7 should be interpreted as rough order-of-magnitude indicators rather than precise predictions. Several sources of uncertainty merit discussion:

- **Traffic concentration:** If the affected port pairs include disproportionately high-volume corridors (e.g., Asia–Europe via Suez), the actual number of affected vessels could be 2–3× higher than our central estimate. Conversely, if the affected pairs are predominantly low-volume routes, the actual number could be lower.
- **Vessel heterogeneity:** Different vessel types respond differently to chokepoint closure. Large container ships and VLCCs (Very Large Crude Carriers) face the highest rerouting costs due to fuel consumption and draft restrictions at alternative routes. Smaller vessels may have more flexibility. Our estimates treat all vessels equally.
- **Dynamic adjustment:** In practice, chokepoint closure would trigger immediate queuing, followed by gradual fleet redeployment to alternative routes. The steady-state number of affected vessels (after adjustment) would differ from the initial impact. Our estimates reflect the steady-state assumption.
- **Temporal variation:** Annual transit counts vary with global trade cycles, seasonal patterns, and geopolitical events. The 2020 COVID-19 pandemic reduced traffic at most chokepoints by 5–15%; conversely, post-pandemic recovery saw record transits at several chokepoints. Our estimates use mid-period averages.

For trade-security assessments, the Suez Canal estimate is particularly policy-relevant. Approximately 19,500 vessels transit the Suez Canal annually, handling roughly 12% of global trade by volume ([Cariou and Cheaitou, 2021](#)). Under our closure scenario, all Suez-dependent traffic must reroute via the Cape of Good Hope or through the Panama Canal, adding a mean of 9,949 km-equivalent to affected routes. The 2021 Ever Given grounding provided a real-world preview of such disruption: even a six-day blockage produced cascading supply-chain effects and measurable increases in shipping costs ([Cariou and Cheaitou, 2021](#); [Verschuur et al., 2023](#)).